Waqar Ahmed Khan

Torque Maximizing and Flux Weakening Control of Synchronous Machines

School of Electrical Engineering

Thesis submitted for examination for the degree of Master of Science in Technology.

Espoo 17.05.2016

Thesis supervisor:

Prof. Marko Hinkkanen

Thesis advisor:

Hafiz Asad Ali Awan, M.Sc. (Tech.)

Aalto University
School of Electrical
Engineering

AALTO UNIVERSITY
SCHOOL OF ELECTRICAL ENGINEERING

ABSTRACT OF THE
MASTER'S THESIS

Author: Waqar Ahmed Khan

Title: Torque Maximizing and Flux Weakening Control of Synchronous Machines

Date: 17.05.2016 Language: English Number of pages:8+55

Department of electrical engineering

Professorship: Electric Drives Code: S-81

Supervisor: Prof. Marko Hinkkanen

Advisor: Hafiz Asad Ali Awan, M.Sc. (Tech.)

In this thesis, the torque maximizing and field weakening control strategies for synchronous machines with magnetically anisotropic structure such as synchronous reluctance machines (SyRMs) and interior permanent magnet machines (IPMs) are studied. In order to obtain maximum torque using minimum stator current, the maximum torque per ampere (MTPA) control strategy is employed below the base speeds. The MTPA control is limited by the maximum available voltage of the motor. Therefore, field weakening (FW) control is employed in order to achieve speeds higher than base speed. To obtain maximum torque while effectively reducing the stator flux at the same time the maximum torque per volt (MTPV) is employed at high speeds. The control techniques are realized using direct flux vector control (DFVC) strategy. Performance of the DFVC technique is analysed in unsaturated and saturated magnetic conditions. Robustness of the technique against parameter variation is evaluated by a series of loading tests. Performance of the DFVC is then evaluated by comparing it with the rotor oriented current vector control. Simulations are performed from experimental data of 7.5 kW IPM drive.

Keywords: Direct flux vector control (DFVC), field weakening (FW), interior permanent-magnet synchronous motors (IPMs), maximum torque per ampere (MTPA), maximum torque per volt (MTPV)

Preface

Firstly, I would like to thank Almighty Allah for providing me with the strength, motivation and perseverance to achieve my goal. It was an arduous road and a fruitful one. Secondly, I would like to express my deepest gratitude to Prof. Marko Hinkkanen for his constant guidance, assistance and for providing me with the opportunity to work under his supervision. It was a learning experience of a lifetime.

I would like to thank my colleagues Mr. Asad Ali Awan, Mr. Maksim Sokolov and Dr. Seppo Saarakkala for their valuable time and for guiding me through this journey. Thank you Mr. Jussi Koppinen and Mr. Mahafugar Rahman for your useful comments and for making the workplace such a cool and fun environment. It would be wrong not to mention all my friends, who have been a constant source of inspiration everyday.

Lastly, I would like to express my deepest love, admiration and gratitude toward my whole family especially my mother. She has been a pillar of support for me in the most crucial times. I dedicate this thesis in memory of my father who is not with us any more. Everything I am is a result of your direction, guidance and love. We love you and miss you Baba.

Espoo, 17.05.2016

Waqar Ahmed Khan

Contents

Symbols and abbreviations

Symbols

Boldface letters represent matrices and vectors. Reference values are marked by the subscript ref.

dq	Synchronous or rotating coordinates
f_s	Sampling frequency
$f\tau$	Flux-torque coordinates
$\boldsymbol{G}_\mathrm{o}$	Observer gain matrix
i_ch	Characteristic current
i_max	Maximum allowed motor current
$\boldsymbol{i}_\mathrm{s}$	Stator current real space vector in synchronous coordinates
i_s	Magnitude of stator current real space vector
$\boldsymbol{i}_\mathrm{s}^{\mathrm{f}\tau}$	Stator current real space vector in $f\tau$ coordinates
i_d	d-axis component of the stator current
i_q	q-axis component of the stator current
i_τ	τ-axis component of the stator current
i_f	f-axis component of the stator current
i_MTPV	MTPV limitation current
$i_{\tau,\mathrm{ref}}$	Reference τ component of stator current
$\boldsymbol{J}$	Orthogonal rotation matrix
J	Total moment of inertia for a system
k_t	Torque factor
$k_\mathrm{p,f}$, $k_{\mathrm{p},\tau}$	Proportional gains of PI controller
$k_\mathrm{i,f}$, $k_{\mathrm{i},\tau}$	Integral gains of PI controller
L_s	Stator inductance
$\boldsymbol{L}_\mathrm{s}$	Inductance matrix
L_d	Direct-axis inductance

L_q	Quadrature-axis inductance
p	number of pole pair
R_s	Stator resistance
t	Time variable
T_e	Electromagnetic torque
$T_\mathrm{e,ref}$	Reference torque-output of speed controller
T_L	Load torque
T_max	Maximum motor torque
T_s	Sampling period
u_dc	DC link voltage
u_d	d-axis component of the stator voltage
u_q	q-axis component of the stator voltage
u_f	f-axis component of the stator voltage
u_τ	τ-axis component of the stator voltage
$\boldsymbol{u}_\mathrm{s}^{\mathrm{f}\tau}$	Stator voltage real space vector in $f\tau$ coordinates
$u_\mathrm{s,max}$	Maximum terminal voltage
$\boldsymbol{u}_\mathrm{s}$	Stator voltage real space vector in synchronous coordinates
u_s	Magnitude of stator voltage real space vector
$\boldsymbol{u}_\mathrm{s,ref}$	Reference voltage-output of the current controller
α	Voltage margin constant
$\alpha\beta$	Stationary or stator coordinates
β	Current angle
δ	Load angle
$\hat{\delta}$	Estimated Load angle
δ_max	Maximum load angle
k	δ dependent parameter
b	δ and ψ_s dependent parameter
ϑ_m	Electrical angle
ψ_d	d-axis component of the stator flux

ψ_{pm}	Permanent-magnet flux
$\boldsymbol{\psi}_{\mathrm{pm}}$	Permanent-magnet flux vector
ψ_{q}	q-axis component of the stator flux
$\boldsymbol{\psi}_{\mathrm{s}}$	Stator flux real space vector in synchronous coordinates
ψ_{s}	Magnitude of stator flux real space vector
$\hat{\psi}_{\mathrm{s}}$	Magnitude of estimated stator flux real space vector
$\psi_{\mathrm{s,ref}}$	Reference stator flux
$\boldsymbol{\psi}_{\mathrm{s}}^{\mathrm{f}\tau}$	Stator flux real space vector in $f\tau$ coordinates
ω_{m}	Electrical angular speed
$\omega_{\mathrm{m,ref}}$	Reference electrical angular speed
ω_{o}	Observer crossover frequency

Abbreviations

1-D	One-dimensional
2-D	Two-dimensional
2DOF	Two-degrees-of-freedom
AC	Alternating current
DC	Direct current
DFVC	Direct flux vector control
DTC	Direct torque control
FW	Field weakening
IPM	Interior permanent-magnet synchronous motor
LUT	Look up table
MTPA	Maximum torque per ampere
MTPV	Maximum torque per volt
PM	Permanent magnet
PI	Proportional integral
PMSM	Permanent-magnet synchronous motor
SyRM	Synchronous reluctance motor

1 Introduction

1.1 Background

Clean, reliable and efficient energy generation with minimum harm to the environment has proven to be quite a substantial challenge. Atmospheric pollution arising from gas emissions by conventional fossil fuel based traction systems contribute significantly to the issue of global warming. These energy issues have driven the focus of automotive industry from the use of conventional internal combustion engine (ICE) propulsion systems towards the promotion of more environmental friendly electric vehicles (EVs) [1–3].

The idea of a propulsion device powered by electricity has been around for almost 200 years. Shortcomings of electric vehicles such as finite driving range (limited battery capacities), high costs and lack of charging facilities have failed to impress the public to be used as a general purpose traction device [4]. Progress halted by such limitations is being overcome by the combination of ICE propulsion systems with electric drive technology that leads to production of hybrid electric vehicles (HEVs). HEVs yield advantages such as reduced fuel consumption, minimum gas emissions and regenerative braking making them highly favourable over ICE technology [5].

Electrical machines are the most vital component in traction applications as they provide the electromechanical energy conversion. Propulsion applications require drive systems that can operate on high torque, power density while reducing maintenance costs and operational losses. Since the beginning of the 20th century, induction machines (IMs) have remained a popular choice in industrial practices owing to high ruggedness and reduced cost (absence of commutators and slip rings). Despite the merits, IMs are still less efficient than another class of AC machines the permanent magnet synchronous machines (PMSMs) [6]. In IMs a part of the rotor flux is produced by the currents flowing in rotor windings while in PMSMs the rotor flux is actually the permanent magnet flux generated by the permanent magnets (PMs) mounted on the rotor structure. Elimination of the rotor cage reduces the rotor mass thus PMSMs have a lower inertia and faster torque response compared with IMs of the same size. Additionally, absence of rotor currents eliminate the rotor

losses leading to more efficient operation. Therefore, PMSMs are a more suitable candidate for traction applications.

PMs used in PMSMs need to have large coercivity and high flux densities. Magnetic materials such as ferrite, NdFeB, AlNiCo are being employed as PMs in the machines. Particularly, ferrite magnets have become the common choice in PMSMs owing to their reduced cost [7]. The control of PMSMs can be divided into two types: sensored and sensor-less control. In sensor-less control, speed can be estimated using estimation algorithms (back-emf based and signal injection) [8]. These techniques tend to be computationally tedious and have limitations at low speeds. In sensored control, PMSMs are provided with an absolute rotor position sensor, e.g., an incremental encoder etc mounted on the rotor shaft. The position sensor increases the gross cost of the drive system but it compensates the set back by providing accurate position information at all speeds [2, 3, 9].

The rotor oriented current control is by far the most common control method employed in traction applications. However, other vector control techniques have also been used. One such technique based on control in the stator flux oriented reference frame is called the direct flux vector control (DFVC) [2, 3, 10–14]. The DFVC allows direct control of stator flux and torque by manipulation of its controlled variables. The technique is closely related to the direct torque control (DTC) in which the torque and flux are controlled directly by manipulation of instantaneous space vectors.

PMSMs can be divided into two categories based on geometrical construction: the surface mounted permanent magnet synchronous machine (SPMs) and interior permanent magnet synchronous machine (IPMs) [3, 15]. In IPMs permanent magnets are buried inside the rotor structure. The magnets are protected against the centrifugal forces leading to a more robust construction. A high reluctance path is encountered by flux along the d-axis compared to q-axis, causing the motor to exhibit magnetic saliency [16]. The inductances vary with the position of rotor and contribute in the producing a part of total torque.

Total torque in an IPMs is a combination of field torque and reluctance torque. The torque produced by the PM flux is known as the field torque while the reluctance torque is produced as a result of magnetic saliency [15]. A particular torque in an IPMs can be generated by theoretically an infinite combination of current vectors in the dq reference frame. However, there exist a particular set of current vectors for every torque that minimizes the stator current magnitude. The operation of the motor on such operating points ensures maximum torque generation, minimum copper loss in stator windings and high efficiency. This control strategy is known as maximum torque per ampere (MTPA) control [9, 16–18]. High speed operation of AC machines requires the weakening of the stator flux [19]. As it was stated earlier, rotor flux of PMSMs is essentially constant. Though the stator flux can be weakened by applying a demagnetizing current along the d-axis [20]. Optimal solution now involves maximizing the output torque while minimizing the stator flux by proper selection of controlled vectors. This control strategy pursued at high speeds is known

as maximum torque per volt (MTPV) control [2,3,9,13]. The control solution is not so trivial in a sense that limitations such as saturation effects, voltage and current limit constraints complicate the selection of optimal current vectors.

1.2 Objective and Outline of the Thesis

The objective of this thesis is to evaluate the performance of the DFVC in unsaturated and saturated magnetic condition. The performance criteria is set to determine how well the DFVC operates with the optimal control strategies as magnetic conditions are varied. The robustness of the DFVC against parameter detuning in the controller is also evaluated. Lastly, the performance of the DFVC is compared with a conventional current scheme to determine optimality in terms of performance.

This thesis is divided into six sections. Section 2 details the structure of PMSMs and motor model in the synchronously rotating reference frame. Literature review on existing MTPA and MTPV control methods is included in section 3. Section 4 consists of literature review on the DFVC technique. Section 5 details the results of simulations carried out in MATLAB/Simulink environment. The conclusions based on results are summarized in section 6.

2 Modelling of a Synchronous Machine

This chapter is focused on discussion of various types of IPMs in literature and its continuous-time modelling employed for control purposes. Magnetically salient pole rotors can be classified into two types based upon the construction. Salient pole machines without PMs in the rotor are called the synchronous reluctance machines (SyRMs) (Fig.2.1(a)) while machines having PMs buried inside the rotor structure are called the interior permanent magnet synchronous machines (IPMs). The salient pole PM rotors can be further classified into machines where either the PMs are placed within the openings on the rotor surface (inset IPMs) (Figure 2.1(b)), buried inside the rotor (buried IPMs) (Figure 2.1(c)) or placed within the hollow flux barriers forming a union of SyRMs and IPMs called the permanent magnet assisted synchronous reluctance machines (PMASyRMs) (Figure 2.1(d)). In each case, the placement of magnets increases the effective air gap length along the direction of PM flux. The relative permeability of PMs is approximately equal to that of the air, $\mu_r = 1.05$. These magnets appear as free space along the flux path giving rise to salient characteristics in the machine.

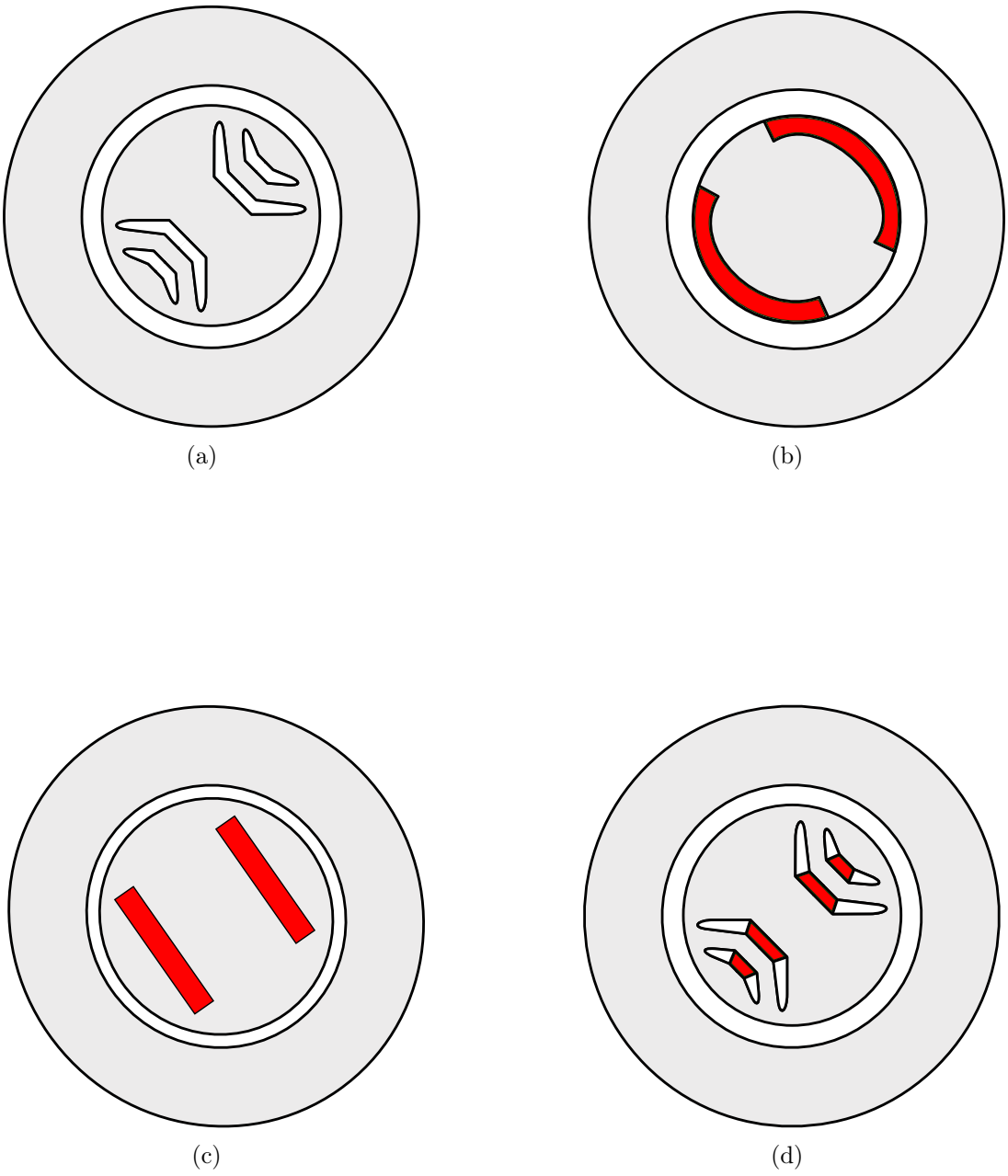

Figure 2.1: Various types of two pole salient machines (a) Synchronous reluctance machine (b) Inset interior permanent magnet synchronous machine (c) Buried interior permanent magnet synchronous machine (d) Permanent magnet assisted synchronous reluctance machine.

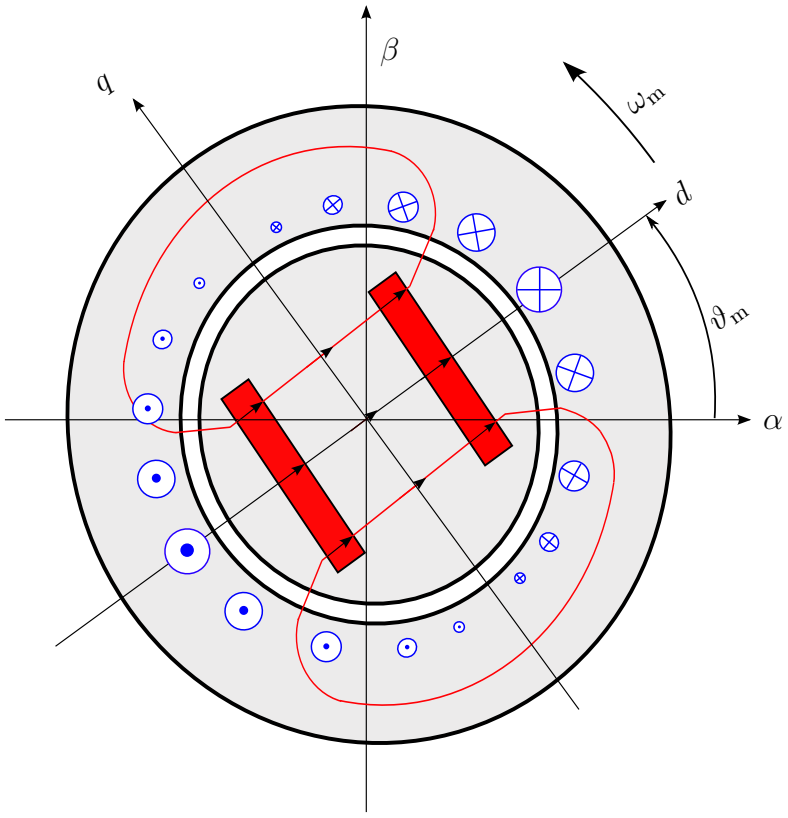

Figure 2.2: Conceptual diagram of a two pole three-phase IPM.

2.1 Continuous Time Modelling of IPMs

Figure 2.2 shows the conceptual diagram of a 3-phase IPM with 3-phase concentrated winding on the stator and buried PMs in the rotor. The terms $\alpha\beta$ represents stationary coordinates while dq represents the synchronous coordinates. The d-axis is aligned with the PM flux vector while the q-axis is displaced from the d-axis by 90 electrical degrees. As seen from Figure 2.2, the d-axis is shifted from α-axis by rotor position angle ϑ_m. The angle ϑ_m being a function of speed is given by,

$$\vartheta_\mathrm{m}(t) = \int \omega_\mathrm{m} \mathrm{d}t \tag{2.1}$$

The dynamic circuit model for IPMs is shown in Figure 2.3. Real valued space vectors will be used for modelling purposes. The voltage equation in rotor coordinates is given by,

$$\boldsymbol{u}_\mathrm{s}(t) = R_\mathrm{s}\boldsymbol{i}_\mathrm{s}(t) + \frac{\mathrm{d}\boldsymbol{\psi}_\mathrm{s}(t)}{\mathrm{dt}} + \omega_\mathrm{m}\boldsymbol{J}\boldsymbol{\psi}_\mathrm{s}(t) \tag{2.2}$$

where $\boldsymbol{u}_\mathrm{s} = [u_\mathrm{d}, u_\mathrm{q}]^T$, $\boldsymbol{i}_\mathrm{s} = [i_\mathrm{d}, i_\mathrm{q}]^T$, $\boldsymbol{\psi}_\mathrm{s} = [\psi_\mathrm{d}, \psi_\mathrm{q}]^T$ are the real valued space vector of stator voltage, stator current and stator flux. The resistance of the stator winding is

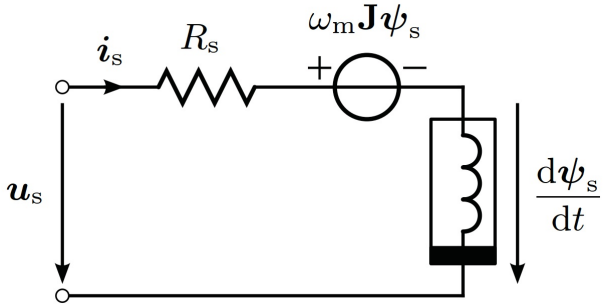

Figure 2.3: Dynamic space vector model of IPMs in rotor coordinates [21].

R_s and $\boldsymbol{J} = \left[\begin{smallmatrix} 0 & -1 \\ 1 & 0 \end{smallmatrix}\right]$ is called the rotation matrix. The inclusion of term t represents that all space vectors are time dependent.

The stator flux equation is defined as,

$$\boldsymbol{\psi}_\mathrm{s}(t) = \boldsymbol{L}_\mathrm{s}\boldsymbol{i}_\mathrm{s}(t) + \boldsymbol{\psi}_\mathrm{pm} \tag{2.3}$$

where $\boldsymbol{\psi}_\mathrm{pm} = \left[\psi_\mathrm{pm}, 0\right]^T$ is the real valued PM flux vector and $\boldsymbol{L}_\mathrm{s} = \left[\begin{smallmatrix} L_\mathrm{d} & 0 \\ 0 & L_\mathrm{q} \end{smallmatrix}\right]$ is the stator inductance in rotor coordinates.

Using (2.3) and (2.2) the voltage equation in component form can be written as,

$$u_\mathrm{d} = R_\mathrm{s} i_\mathrm{d} - \omega_\mathrm{m}\psi_\mathrm{q} + \frac{\mathrm{d}\psi_\mathrm{d}}{\mathrm{d}t} \tag{2.4a}$$

$$u_\mathrm{q} = R_\mathrm{s} i_\mathrm{q} + \omega_\mathrm{m}\psi_\mathrm{d} + \frac{\mathrm{d}\psi_\mathrm{q}}{\mathrm{d}t} \tag{2.4b}$$

where the d and q components of $\boldsymbol{\psi}_\mathrm{s}$ in component form are given as,

$$\psi_\mathrm{d} = L_\mathrm{d} i_\mathrm{d} + \psi_\mathrm{pm} \tag{2.5a}$$

$$\psi_\mathrm{q} = L_\mathrm{q} i_\mathrm{q} \tag{2.5b}$$

The magnitude of the stator voltage, current and flux vector are given as,

$$u_\mathrm{s} = \sqrt{u_\mathrm{d}^2 + u_\mathrm{q}^2} \tag{2.6}$$

$$i_\mathrm{s} = \sqrt{i_\mathrm{d}^2 + i_\mathrm{q}^2} \tag{2.7}$$

$$\psi_\mathrm{s} = \sqrt{\psi_\mathrm{d}^2 + \psi_\mathrm{q}^2} \tag{2.8}$$

The model described above is valid for both SPMs and SyRMs. By insertion of L_s = L_d =L_q the described model is transformed to that of a SPM and by setting ψ_pm = 0, the model is reduced to that of a SyRM.

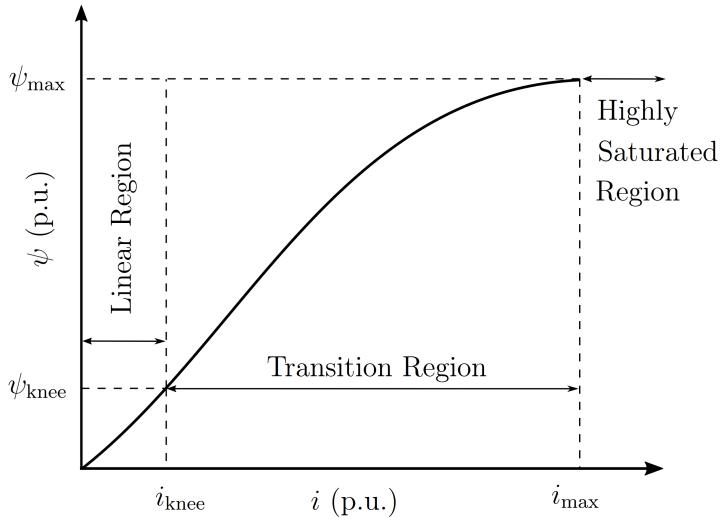

Figure 2.4: Typical saturation characteristics of an inductor [22].

2.2 Magnetic Saturation

Ferromagnetic materials used as core materials in electrical machines have an inherent ability to saturate as the flux passing through the core is increased. Saturation phenomenon in an inductor can be analogized to a rotating machine with ease. The flux linkage-current relationship of an inductor is shown in Figure 2.4. The curve is divided into three regions of operation. Referring to Figure 2.4 in the area of low excitation, the flux-current relationship is linear and saturation is non-existent. The inductance of the inductor retain its nominal unsaturated value. The region is known as the linear or unsaturated region. After a particular value of flux known as the knee point (ψ_{knee}) is reached and saturation in the core begins to take place, i.e., the flux-current relationship becomes non-linear. In this transition zone with the increase of current the permeability of inductor drops and the rate of change of flux decreases. Therefore, saturation effectively decreases the inductance with increasing current. Lastly, in the end region the flux is almost constant and equal to its maximum value. This is known as the highly saturated region. As seen in Figure 2.4 the flux retains its constant value for in this zone [22].

To realize high torque requirements, silicon steel cores are operated in the region of high saturation [23]. As discussed, the inductances L_d and L_q cannot be assumed as constant parameters during the entire operation of the machine. Saturation effects have to be taken into account in the motor model and in the controller to accurately simulate the real-time machine behaviour. The saturation effects in this study are taken into using an explicit function. The motivation behind using functions are : (1) Defined range is virtually unbounded (2) Data storage is not required. More information is given in section 5.

2.3 Torque Production in IPMs

The torque equation of an IPM is given as,

$$T_{\mathrm{e}} = \frac{3p}{2} \boldsymbol{i}_{\mathrm{s}}^{\mathrm{T}} \boldsymbol{J} \boldsymbol{\psi}_{\mathrm{s}} \tag{2.9}$$

where p is the number of pole pair in the machine and T represents the transpose of the current vector $\boldsymbol{i}_{\mathrm{s}}$. The above equation can be simplified by considering (2.3), (2.5) as

$$T_{\mathrm{e}}(i_{\mathrm{d}}, i_{\mathrm{q}}) = \frac{3p}{2} \left[\psi_{\mathrm{d}}(i_{\mathrm{d}}, i_{\mathrm{q}}) i_{\mathrm{q}} - \psi_{\mathrm{q}}(i_{\mathrm{d}}, i_{\mathrm{q}}) i_{\mathrm{d}} \right] \tag{2.10}$$

3 MTPA and Field Weakening Control

The total losses in the motor consist of the iron losses, copper losses (in the winding) and stray losses. The copper losses are the most dominant ones below base speed ω_B while the iron losses grow significantly as the speed is further increased [9]. This chapter reviews a current minimizing strategy for reducing the copper losses called the maximum torque per ampere (MTPA) control. The lack of available terminal voltage above ω_B presents a limitation to the MTPA control. Therefore, the control strategy needs to be modified in order to extend the operating range, thus gaining access to high speeds while keeping the losses minimum as possible. The control is termed as field weakening control. The chapter discusses the aforementioned control strategies while keeping into account following assumptions

- A linear or constant parameter steady state model of synchronous machines discussed in the section 2 is assumed. Thus, inductance variation due to saturation and cross-saturation effects is ignored. The stator resistance and PM flux variations are also assumed to remain constant in the entire operating range.
- The motor is supplied via an inverter having limited current and voltage rating.

3.1 Motor Limits

Practical drives system are fed through a power electronic converters that impose a limit on the maximum output voltage and current that the inverter can produce.

3.1.1 Current Limit:

The current limit i_{max} depends on the motor construction. It is decided by factors, e.g., thermal dissipation, cooling methods and the available output current of the inverter. Taking current limit into account (2.7) is modified to,

$$\sqrt{i_d^2 + i_q^2} = i_s \leq i_{max} \tag{3.1}$$

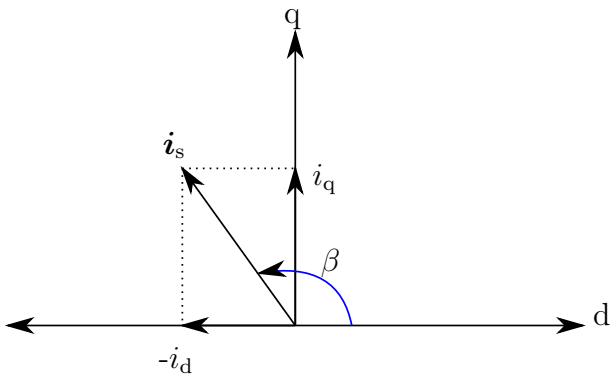

Figure 3.1: Current angle.

In the i_d-i_q domain current limit constraint takes the form of a circle having a center at origin with a radius of i_{max}.

3.1.2 Voltage Limit:

Neglecting the ohmic drop across resistance R_s the voltage limit is represented by equation,

$$\frac{\left(i_d + \frac{\psi_{pm}}{L_d}\right)^2}{L_q^2} + \frac{(i_q)^2}{L_d^2} \leq \left(\frac{u_{s,max}}{\omega_m L_d L_q}\right)^2 \tag{3.2}$$

where $u_{s,max} = u_{dc}/\sqrt{3}$ with u_{dc} being the DC link voltage. Within the i_d-i_q plane the voltage limit takes the form of an ellipse having a center at $(\psi_{pm}/L_d,0)$. The ellipse encloses all the operating points where the terminal voltage does not exceed the maximum voltage [24]. All i_d-i_q current pairs that exist on or within the intersection of voltage ellipse and current circle are the allowable points of operation at any speed.

3.2 Maximum Torque Per Ampere Control

The copper losses being a function of stator current increase with the torque. HEV applications have large torque demands at low speed for purpose of fast acceleration and deceleration [25]. These requirements point towards the use of control technique that maximizes the torque while making use of as minimum stator current as possible. The control strategy is known as maximum torque per ampere control (MTPA) and is used for minimum loss operation under ω_B [9, 16, 26]. Bearing in mind the assumptions taken and using (2.5) in (2.10), the torque equation is given as

$$T_e = \frac{3p}{2}\left[\psi_{pm} i_q + (L_d - L_q) i_d i_q\right] \tag{3.3}$$

We infer from the derived equation that the torque of an IPM is a combination of two components. The torque produced by the product $\psi_{pm} i_q$ known as field torque while

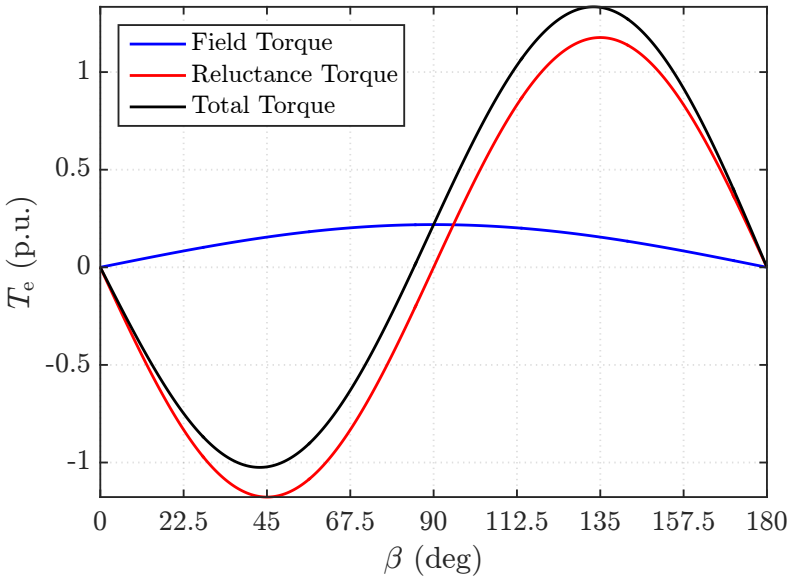

Figure 3.2: Current angle versus produced torque.

the torque produced as a result of magnetic saliency ($L_d \neq L_q$) called reluctance torque. As shown in Figure 3.1 the current vector $\boldsymbol{i}_s$ is displaced from d-axis by an angle β. Resolving the current vector to its orthogonal components we get,

$$i_d = i_s \cos\beta \tag{3.4a}$$
$$i_q = i_s \sin\beta \tag{3.4b}$$

where β is known as the current angle. Substituting (3.4) in (3.3) we obtain,

$$T_e = \frac{3p}{2}\left[\psi_{pm} i_s \sin\beta + (L_d - L_q) i_s^2 \frac{\sin 2\beta}{2}\right] \tag{3.5}$$

The variation of current angle β versus the produced torque components is shown in Figure 3.2. The simulated machine is an IPM whose ratings are provided in section 5. Taking partial derivative of (3.5) with respect to the current angle and setting it equal to 0 provides the maximum torque that can be produced by a particular current angle,

$$\frac{\partial T_e}{\partial \beta} = \frac{3p}{2}\left[\psi_{pm} i_s \cos\beta + (L_d - L_q) i_s^2 \cos 2\beta\right] = 0 \tag{3.6}$$

Substitution of (3.4) in (3.6) results in,

$$(L_d - L_q) i_d^2 + \psi_{pm} i_d + (L_d - L_q) i_q^2 = 0 \tag{3.7}$$

The equation stated above provides i_d-i_q current references for MTPA control of an IPM motor. We can see that with the assumed dq axis alignment, the current angle

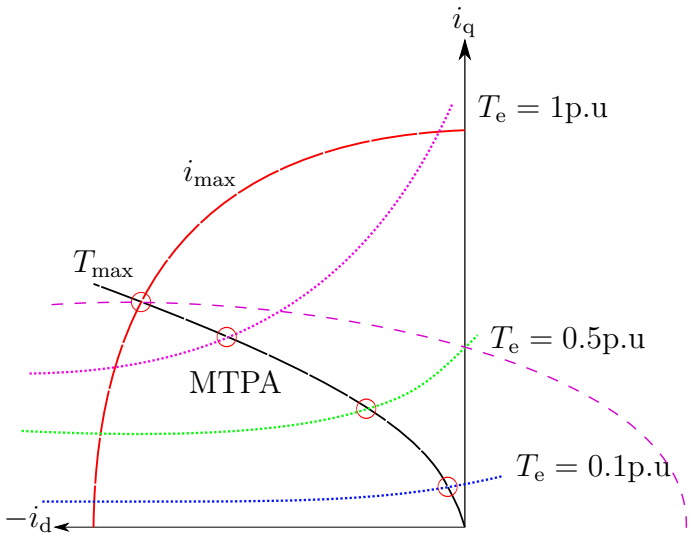

Figure 3.3: Circle diagram exhibiting MTPA trajectory, torque curves, voltage ellipse and current limit.

needs to be greater than 90 degrees for positive torque production (Figure 3.1). This points towards the use of negative i_d current reference. Figure 3.3 shows an i_d-i_q plane depicting voltage and current limits for a typical IPM motor. The solution of (3.7) results in current data points that make up the MTPA trajectory. The torque equation (3.3) is represented as dotted hyperbolas in the plane. The i_d-i_q current pairs that make up such hyperbolas produce the same torque. Intersection of the torque and MTPA curve (indicated by red circles in Figure 3.3) within the current and voltage limit represents the most optimal current references to produce that particular torque. In other words, operating on these current references ensures minimum stator current usage while producing a particular torque. It should be noted that if voltage considerations are not taken into account, the MTPA operation is limited only by current limit i_{max}. The intersection of the torque and the MTPA curve at the i_{max} limit produces maximum torque T_{max} of a given motor.

3.3 Field Weakening Control

In addition to high torque requirements at low speeds, traction applications require drive systems that provide constant power at high speeds [14]. The drive must be able to maintain the constant power over a wide speed range [13, 27]. The speed of the motor increases with the terminal voltage up until the base speed. At base speed the terminal voltage saturates to its maximum value. The speed of the motor cannot be increased any further unless a proper control strategy is implemented to reduce the stator flux. If a demagnetizing magnetomotive force (MMF) generated by manipulation of stator currents is applied, the apparent MMF generated by PMs could be reduced and the motor speed will increase. The strategy is known as field-weakening (FW). Figure 3.5(b) show the typical torque speed characteris-

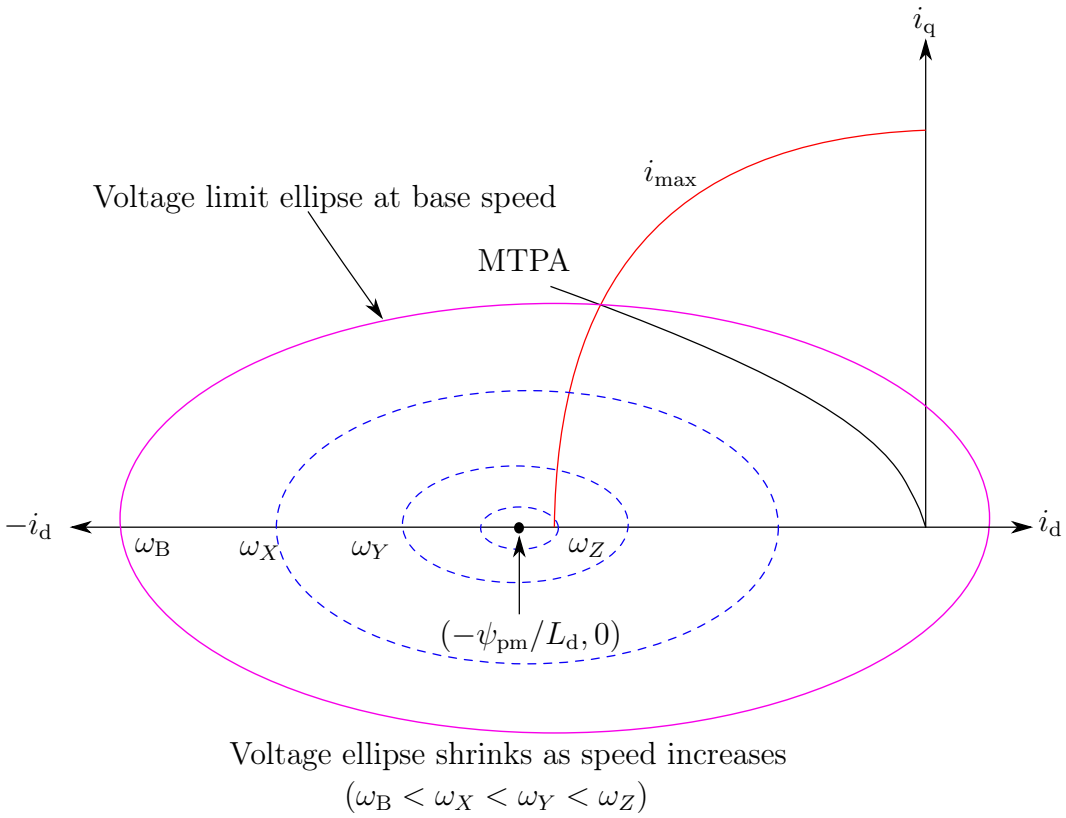

Figure 3.4: Circle diagram exhibiting MTPA trajectory, current limit and voltage limits.

tics of an IPM motor. In the constant torque region, the motor is accelerated by the maximum torque using the MTPA control up until the base speed (ω_m=ω_B). As a result of voltage constraints, ω_B is the maximum achievable speed by torque produced through MTPA control. Beyond ω_B, FW control takes over resulting in a simultaneous decrease in torque and an increase in speed. It should be noted here that unlike in the MTPA control where the torque is only subjected to the current limit constraints, both the voltage and current constraints limit the torque production during the FW region.

It is evident from Figure 3.4 that as the speed of the motor increases, the voltage ellipse shrinks towards its center at (ψ_{pm}/L_d,0). The current references derived from from the MTPA calculations are incapable of satisfying both the current and voltage constraints above the base speed. Therefore, new current references are now derived by simultaneous solution of current limit (3.1) and the voltage limit (3.2),

$$(L_d^2 - L_q^2)i_d^2 + (2\psi_{pm}L_d)i_d + \left(L_q^2 i_s^2 + \psi_{pm}^2 - \frac{u_{s,max}^2}{\omega_m^2}\right) = 0 \tag{3.8}$$

The equation stated above provides the current references in the voltage and current limited FW region. PM drives can be classified into two types based on their speed capabilities. The distinction comes from the comparison of drives characteristic

current i_{ch} and drives maximum current i_{max} [13].

$$i_{\mathrm{ch}} = \frac{\psi_{\mathrm{pm}}}{L_{\mathrm{d}}}$$

3.3.1 Finite Speed Drives

The drives having $i_{\mathrm{ch}} > i_{\mathrm{max}}$ are known as finite speed drives. Such drives have an extensive constant-power speed range which means they are able to achieve very high speeds using a proper FW control strategy. The operation of a finite speed drive from zero to maximum speed is shown in Figure 3.5. The motor is accelerated during speed interval 0-ω_1 by torque T_{e}=T_{N} through current references generated by the MTPA control. This is indicated by trajectory O-A in the torque speed curve (Figure 3.5(b)). It should be noted that the motor is limited to produce rated torque at rated current. However the motor is still capable of producing maximum torque, i.e., at the tangential intersection of i_{max} limit and torque hyperbola indicated by point X in the diagram.

The speed increases with the voltage and beyond $u_{\mathrm{s,max}}$, the FW control takes over. The stator flux is reduced to increase the speed. Current references (given by (3.8)) are now selected by intersection of the rated torque curve and the voltage limit. This is indicated by the region A-B in Figure 3.5(b). Current references cannot be obtained beyond point B by moving on the torque locus because of i_{max} limit. The maximum torque is now determined by the intersection of both the voltage and the current limit indicated by trajectory B-D in the diagram. The FW algorithm decreases the output torque to increase the motor speed beyond ω_2. The decrease results in an increase in power indicated by trajectory B-C in power speed characteristics as shown in the Figure 3.5(c). Point D indicates that the maximum speed has been reached as the current and voltage limits are tangential to each other. Any further increase in speed is now impossible without violating either constraints [24].

3.3.2 Infinite Speed Drives

Drives having $i_{\mathrm{ch}} < i_{\mathrm{max}}$ are known as infinite speed drives. Theoretically, such drives have no upper speed limit and as the name indicates are able to achieve infinite speeds under lossless conditions. Such drives need to obey the maximum torque per voltage (MTPV) limit at high speeds.

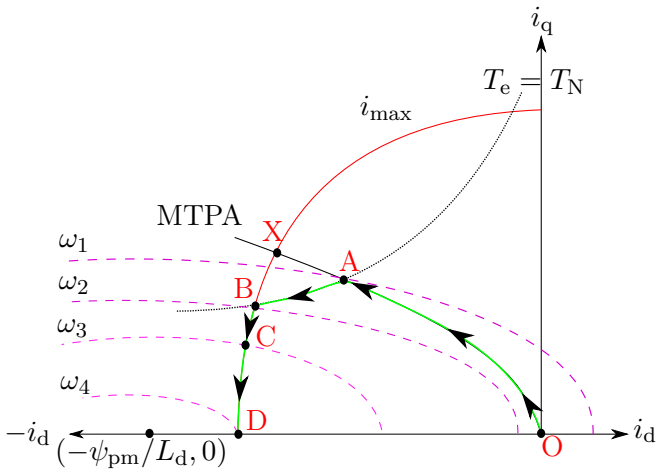

(a)

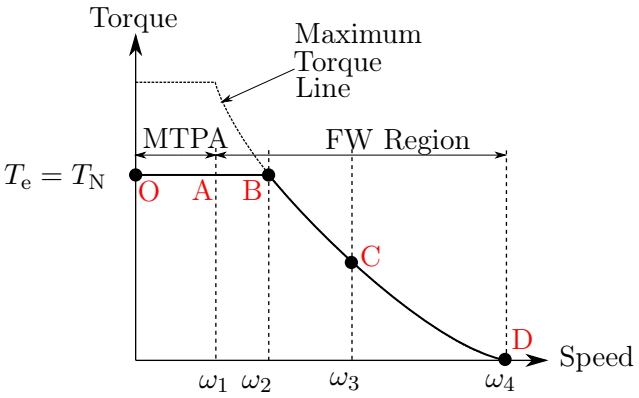

(b)

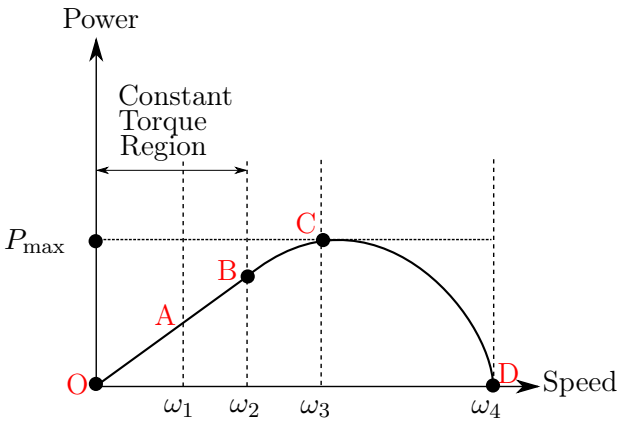

(c)

Figure 3.5: (a) Trajectory of current vectors using the MTPA and the FW control in finite speed IPMs (b) Torque vs speed characteristics (c) Power vs speed characteristics.

3.4 Maximum Torque Per Volt Control

The MTPV operation occurs at very high speeds for an infinite speed drive system in the FW region. Keeping the voltage limit in mind, after particular speed has been reached maximum torque cannot be obtained by exploiting full inverter current [3]. In such a condition, current references are derived based on tangential intersection between the torque curves and the shrinking voltage ellipses. Simultaneous solution of (2.5), (2.8) and (3.3) results in,

$$T_{\mathrm{e}} = \frac{3p}{2}\left[\psi_{\mathrm{d}}\left(\frac{1}{L_{\mathrm{q}}} - \frac{1}{L_{\mathrm{d}}}\right) + \frac{\psi_{\mathrm{pm}}}{L_{\mathrm{d}}}\right]\sqrt{\psi_{\mathrm{s}}^2 - \psi_{\mathrm{d}}^2} \tag{3.9}$$

Taking partial derivative of (3.9) with respect to ψ_{d} and setting it equal to 0 provides the maximum torque during the MTPV operation,

$$\frac{\partial T_{\mathrm{e}}}{\partial \psi_{\mathrm{d}}} = 0$$

Simplification leads to,

$$(\psi_{\mathrm{pm}} + L_{\mathrm{d}} i_{\mathrm{d}})^2 + \frac{L_{\mathrm{q}}}{L_{\mathrm{d}} - L_{\mathrm{q}}}\psi_{\mathrm{pm}}(\psi_{\mathrm{pm}} + L_{\mathrm{d}} i_{\mathrm{d}}) - (L_{\mathrm{q}} i_{\mathrm{q}})^2 = 0 \tag{3.10}$$

The equation stated above provides the current references in the MTPV region. The MTPV limit similar to the MTPA limit is a hyperbola in the i_{d}-i_{q} plane for an IPM machine [24]. Upto point C (shown in Figure 3.6) the behaviour of an infinite speed IPM drive is exactly similar to a finite speed drive. The MTPV limitation is activated at point C and the optimal current references are now selected by solution of (3.10) . During the MTPV operation, the input current of the drive is lower than the rated current while voltage is limited to $u_{\mathrm{s,max}}$. The output power of the drive (shown in Figure 3.6(c)) falls inversely with the speed and is very small at very high speeds [24]. If the drive is assumed lossless the speed increases constantly until it reaches infinity, as the stator current contour asymptotes to the point ($\psi_{\mathrm{pm}}/L_{\mathrm{d}}$,0) in the i_{d}-i_{q} plane.

Maximizing the torque equation itself is not such as a simple task as it is a constrained optimization problem with constraints being imposed by current and voltage limits. Non-linearities such as saturation phenomenon further complicate the optimization process in practical situations. Early research resorted to optimizing the torque equation by assuming the constant parameter magnetic model [16, 28]. The MTPA and FW solutions were either implemented through the use of look up tables or by approximated polynomial functions. The inclusion of saturation effects via recursive algorithms improved the control performances [9, 20, 26, 29, 30]. A different approach to loss minimization deals with varying the operation point online on torque curves to search for the operation point that results in minimum current or flux magnitude [31–33]. Such techniques are slow converging, model dependent and difficult to implement online.

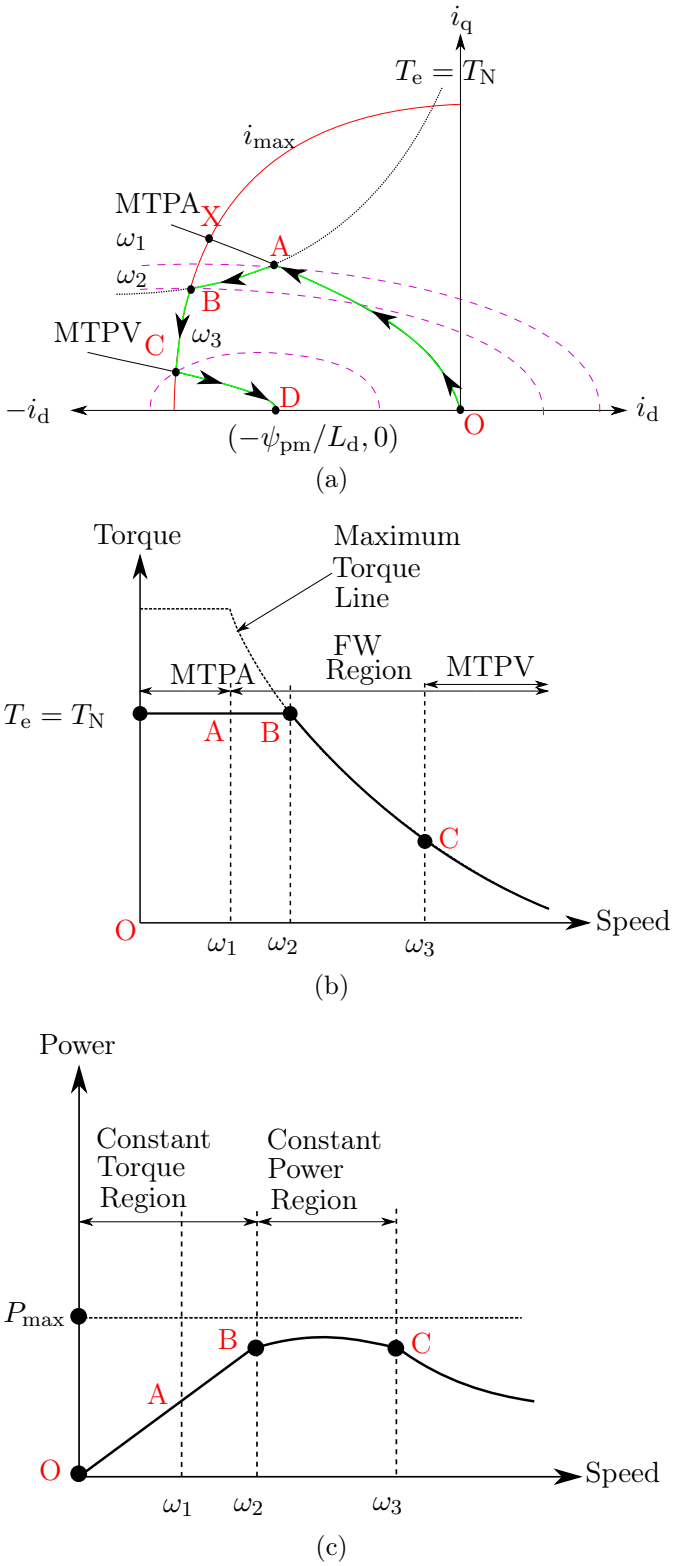

Figure 3.6: (a) Trajectory of current vectors using the MTPA and the FW control in infinite speed IPMs (b) Torque vs speed characteristics (c) Power vs speed characteristics.

4 Direct Flux Vector Control

The direct flux vector control (DFVC) is a control strategy suited for applications that operate in deep FW regions e.g., spindle drives, traction applications [2, 3, 12]. As explained in former section, the FW operation in the dq coordinate system is achieved by usage of a more negative i_d current reference with d-axis aligned in the direction of PM flux. The implementation of the FW in such current control techniques is highly parameter dependent and performance depend on how accurately the motor parameters are identified. The DFVC allows control of the stator flux by direct manipulation of the stator flux vector. The approach has virtually no dependence on the magnetic model making the control more robust [10]. This chapter reviews DFVC strategy incorporating both MTPA and MTPV control in detail.

4.1 DFVC Preliminaries

The DFVC is implemented in flux-torque ($f\tau$) reference frame with the stator flux vector oriented along the direction of the f-axis. The torque axis (τ) is displaced from the f-axis by an angle of electrical 90° as shown in Figure 4.1 while the f-axis leads the d-axis by an angle δ called the load angle. The control variables as described in [10] are either ψ_s and δ or ψ_s and torque current i_τ (projection of current vector $\boldsymbol{i}_\mathrm{s}^{\mathrm{f}\tau}$ along the torque axis). The transformation of voltage, current and flux vectors from the dq to the $f\tau$ reference frame using Park's transformation is,

$$\boldsymbol{u}_\mathrm{s} = e^{\boldsymbol{J}\delta}\boldsymbol{u}_\mathrm{s}^{\mathrm{f}\tau} \tag{4.1a}$$

$$\boldsymbol{i}_\mathrm{s} = e^{\boldsymbol{J}\delta}\boldsymbol{i}_\mathrm{s}^{\mathrm{f}\tau} \tag{4.1b}$$

$$\boldsymbol{\psi}_\mathrm{s} = e^{\boldsymbol{J}\delta}\boldsymbol{\psi}_\mathrm{s}^{\mathrm{f}\tau} \tag{4.1c}$$

where $\boldsymbol{u}_\mathrm{s}^{\mathrm{f}\tau} = [u_\mathrm{f}, u_\tau]^T$, $\boldsymbol{i}_\mathrm{s}^{\mathrm{f}\tau} = [i_\mathrm{f}, i_\tau]^T$, $\boldsymbol{\psi}_\mathrm{s}^{\mathrm{f}\tau} = [\psi_\mathrm{s}, 0]^T$.

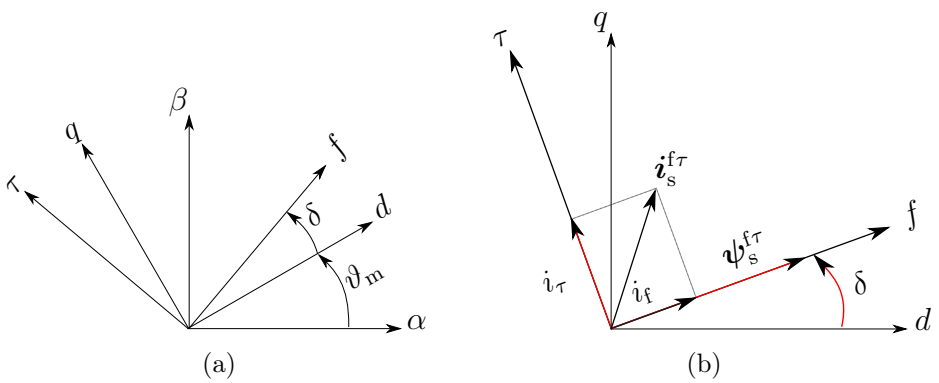

Figure 4.1: (a) Flux torque ($f\tau$) reference frame; (b) Vector diagram in $f\tau$ frame with state variables (marked in red).

Using (4.1), the voltage equation of the motor in $f\tau$ components is given as

$$u_\mathrm{f} = i_\mathrm{f} R_\mathrm{s} + \frac{\mathrm{d}\psi_\mathrm{s}}{\mathrm{d}t} \tag{4.2a}$$

$$u_\tau = i_\tau R_\mathrm{s} + \psi_\mathrm{s}\left(\omega_\mathrm{m} + \frac{\mathrm{d}\delta}{\mathrm{d}t}\right) \tag{4.2b}$$

4.2 State Variable Selection

4.2.1 State Variables (ψ_s,δ)

It can be seen that the u_f voltage loop is completely decoupled from u_τ voltage loop and stator flux ψ_s can be regulated by the manipulation of u_f voltage component directly. Inspection of τ loop indicates that the load angle δ can be regulated by means of u_τ voltage component but there is dynamic interaction with the u_f voltage loop through the term $\psi_\mathrm{s}\omega_\mathrm{m}$. Using equation (4.1) and (3.3), the torque in $f\tau$ reference frame is given as,

$$T_\mathrm{e} = \frac{3p}{2}\frac{1}{L_\mathrm{d}}\left[\psi_\mathrm{s}\psi_\mathrm{pm}\cos\delta + \psi_\mathrm{s}^2\frac{\sin 2\delta}{2}\left(\frac{L_\mathrm{d} - L_\mathrm{q}}{L_\mathrm{q}}\right)\right] \tag{4.3}$$

The equation (4.3) shows that the stator flux and torque can be manipulated by coordinated control of state variables ψ_s and δ. We can see that the torque equation is highly model dependent and complex in terms of control.

4.2.2 State Variables (ψ_s,i_τ)

The control can be made linear and completely model independent by representing the torque as a function of ψ_s and i_τ [2, 3, 11–14]. Torque relationship modified by

using (2.10) and (4.1) in (4.4). The trivial equation suggests the selection of stator flux amplitude ψ_s and current component i_τ as state variables. This allows stator flux control by manipulation of ψ_s while the torque of motor is controlled by current reference i_τ. The flux vector control is employed in direct torque control (DTC) and control of torque through the current component is typical in *dq* current control strategies. Therefore, DFVC can be viewed as union of both the control strategies. Furthermore, there is no limitation on state variable selection as either one of the two choices can be selected for control purposes [10].

$$T_\mathrm{e} = \frac{3p}{2}\psi_\mathrm{s} i_\tau \tag{4.4}$$

Further manipulation of (4.2b) by introducing (4.4) leads to voltage equations into adopted state variables,

$$\frac{\mathrm{d}\psi_\mathrm{s}}{\mathrm{d}t} = u_\mathrm{f} - i_\mathrm{f} R_\mathrm{s} \tag{4.5a}$$

$$\frac{\mathrm{d}i_\tau}{\mathrm{d}t} = \frac{k}{L_\mathrm{d}}(u_\mathrm{f} - i_\mathrm{f} R_\mathrm{s}) + \frac{b}{L_\mathrm{d}}(u_\tau - i_\tau R_\mathrm{s} - \omega_\mathrm{m}\psi_\mathrm{s}) \tag{4.5b}$$

where

$$k = k(\delta) = -\frac{1}{2}\left(1 - \frac{L_\mathrm{d}}{L_\mathrm{q}}\right)\sin 2\delta \tag{4.6}$$

$$b = b(\psi_\mathrm{s}, \delta) = \frac{\psi_\mathrm{pm}}{\psi_\mathrm{s}}\cos(\delta) - \left(1 - \frac{L_\mathrm{d}}{L_\mathrm{q}}\right)\cos 2\delta \tag{4.7}$$

while the inspection of (4.3) reveals that b is also related to T_e by,

$$b(\psi_\mathrm{s}, \delta) = \frac{L_\mathrm{d}}{\psi_\mathrm{s}^2}\left(\frac{\partial T_\mathrm{e}}{\partial \delta}\right)_{\psi_\mathrm{s}=\text{constant}} \tag{4.8}$$

Referring to the voltage equation in controlled variables (4.5), the ψ_s-loop is completely decoupled from the i_τ-loop just as in (4.2a). However, i_τ-loop is coupled to ψ_s-loop through variable k and b. As indicated in (4.6) and (4.7) the variables are functions of flux angle δ and flux component ψ_s and impact the system stability to a great extent.

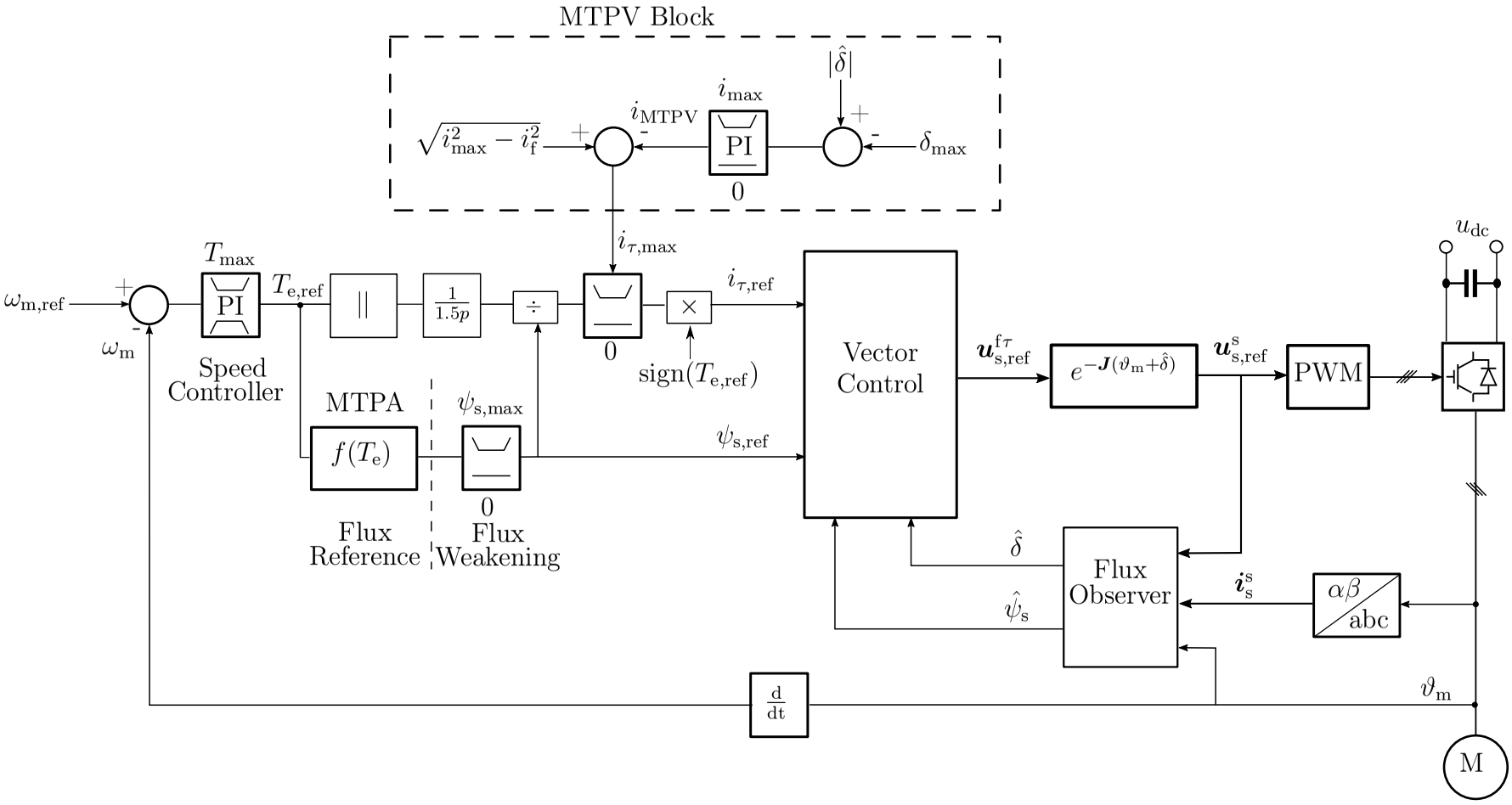

Figure 4.2: Control scheme of the DFVC.

4.3 Control Scheme for DFVC.

The control scheme for the DFVC as presented in [12] is shown in Figure 4.2. The speed regulator is a PI controller that generates the torque reference $T_{\mathrm{e,ref}}$ based on the error between the commanded speed and actual speed. The flux reference $\psi_{\mathrm{s,ref}}$ is generated through the MTPA LUT using $T_{\mathrm{e,ref}}$. The flux weakening block limits the generated flux above ω_{B} (before i_τ is calculated). Current reference i_τ is generated using (4.4). Individual control schemes blocks are explained in the following subsections.

4.3.1 ψ_{s} Reference Generation

The optimal flux reference $\psi_{\mathrm{s,ref}}$ for the generated torque command $T_{\mathrm{e,ref}}$ is determined by the MTPA block containing a 1-D LUT. The LUT is constructed by the manipulation of motor magnetic characteristics. For optimal control of real machines, saturation phenomenon cannot be ignored. The inclusion of saturation in the motor complicates the problem by introducing non-linearity in the motor magnetic model. The MTPA considering saturation of the motor is now determined by the procedure defined in Figure 4.3.

The technique is based on manipulation of experimental data. The motor under test can be identified by procedure, e.g., presented in [34]. The dq-axes current and flux matrices obtained from experimental data are utilized to construct a 3-D torque and current amplitude surface using (2.10) and (2.7). The contours produced by the torque surface are the actual torque hyperbolas on which stator current needs to minimized. The contours produced by the current amplitude surface take the form of a circle, i.e., current limits in the i_{d}-i_{q} plane. Data points in the form of i_{d} and i_{q} that make up the contours of current limits are identified for current levels from 0-i_{max}. Data points for a specific current level are then 2-D interpolated over the torque surface. Hence, we obtain a torque matrix for every interpolated i_{d}-i_{q} current pair in which stator current remains constant while torque varies. The maximum torque is determined from the torque matrix and the current pairs that produce it. These current pairs are the desired MTPA points of operation for the obtained maximum torque. The procedure is repeated for the entire range of current level to obtain the MTPA points for torque range 0-T_{max}. These data points are then 2-D interpolated over ψ_{d} and ψ_{q} maps to obtain the MTPA points of operation in the form of ψ_{d} and ψ_{q}. The optimal stator flux reference is then generated by utilizing the ψ_{d} and ψ_{q} data points through equation (2.8). Implementation of the MTPA is accomplished by using a 1-D LUT with torque as independent quantity and stator flux as the dependent quantity. It should be noted here that the explained procedure takes into account both the saturation and cross saturation effects in the machine since it is based on exploiting actual experimental motor data. The accuracy of this approach depends on how accurately the motor is identified. Figure 4.4 compares the MTPA trajectory in unsaturated and saturated conditions for an IPM motor.

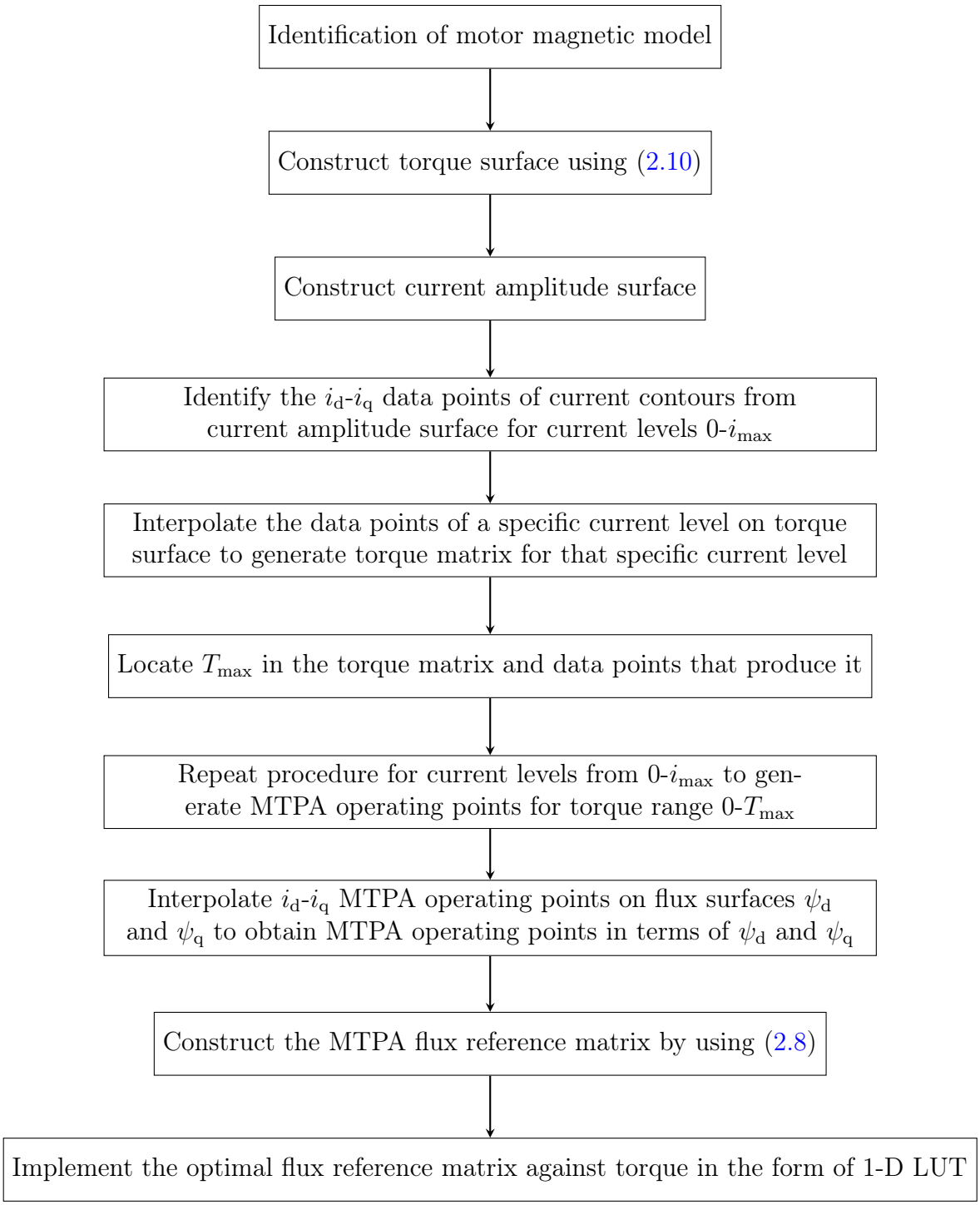

Figure 4.3: Flow diagram of optimal flux reference calculation process.

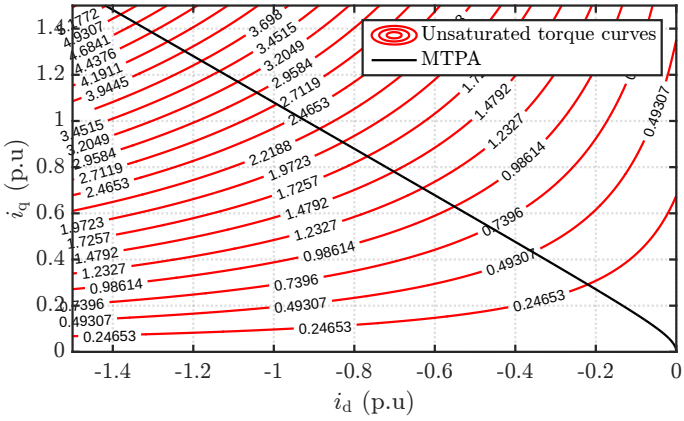

(a)

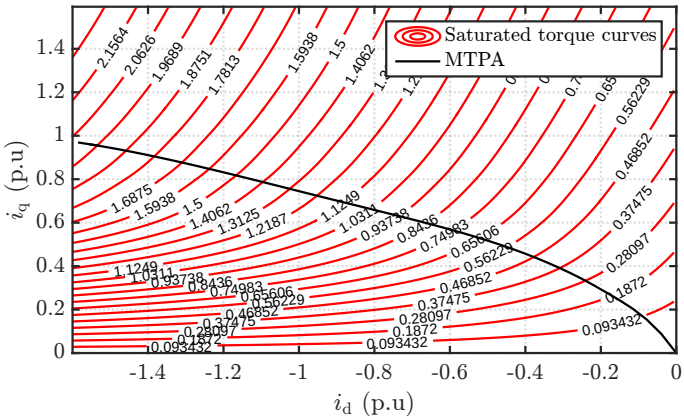

(b)

Figure 4.4: Comparison of the MTPA in unsaturated and saturated conditions.

4.3.2 Flux Weakening

Direct control of the stator flux vector allows simplified flux weakening control algorithms to be used in the scheme. The flux weakening is achieved by,

$$\psi_{\mathrm{s,max}} \leq \alpha \frac{u_{\mathrm{s,max}}}{|\omega_{\mathrm{m}}|} \tag{4.9}$$

where $u_{\mathrm{s,max}} = u_{\mathrm{dc}}/\sqrt{3}$ is dependent on the DC link voltage and α is a term equal or nearly equal to unity. It defines the available voltage margin within the flux and current regulator [2]. In case of low power motors the resistive drops within the stator winding needs to be taken into account and (4.9) is modified to,

$$\psi_{\mathrm{s,max}} = \frac{u_{\mathrm{s,max}} - i_{\tau} R_{\mathrm{s}}}{|\omega_{\mathrm{m}}|} \tag{4.10}$$

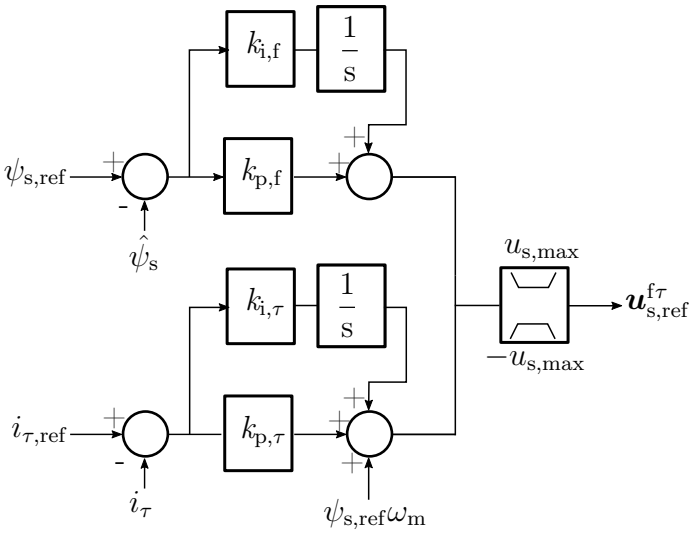

Figure 4.5: ψ_{s} and i_{τ} PI regulators.

4.3.3 i_{τ} Reference Generation

As shown in Figure 4.2, the current reference is generated using saturated reference flux by equation (4.4). Saturation of $i_{\tau,\mathrm{ref}}$ is needed to keep the current vector inside the i_{max} limit. The limit on $i_{\tau,\mathrm{ref}}$ is given by,

$$i_{\tau,\mathrm{ref}} = \sqrt{i_{\mathrm{max}}^2 - i_{\mathrm{f}}^2} \tag{4.11}$$

4.4 Vector Control

The vector control block consist of two PI regulators for ψ_{s} and i_{τ} that provide voltage reference in $f\tau$ coordinates [11].

4.4.1 ψ_{s} Regulator

Referring to (4.5a), the stator flux is directly controlled by u_{f} voltage component with zero interference from the i_{τ} loop. The flux loop response is very fast, apart from the limitation due to PWM time discretization. The flux bandwidth is limited only by the dynamics of the the flux estimator [2]. The regulator is tuned according to the simple internal model control (SIMC) approach [35]. An advantage of this approach is that only a single parameter needs to be tuned. The gains for the flux

regulator are given as,

$$k_{\mathrm{p,f}} = \frac{1 + T_{\mathrm{s}}/3}{T_{\mathrm{c,f}} + T_{\mathrm{s}}} \tag{4.12}$$

$$k_{\mathrm{i,f}} = \frac{1 + T_{\mathrm{s}}/3}{4(T_{\mathrm{c,f}} + T_{\mathrm{s}})} \tag{4.13}$$

where the parameter $T_{\mathrm{s}} = 1/f_{\mathrm{s}}$ is the sampling period and f_{s} is the sampling frequency. The desired response can be obtained by tuning of the factor $T_{\mathrm{c,f}}$. It should be noted that the gains of flux regulator are independent of machines magnetic model and thus independent of saturation effects.

4.4.2 i_τ Regulator

The control of i_τ variable is obtained with the u_τ voltage component with less ideal properties with respect to ψ_{s}. The interaction with the flux loop through the dynamic k and b variables (dependent on the machine magnetic state) introduces a non-linearity in the i_τ control as given in (4.5b). The non-linearities are most visible during transient conditions [3] and can be appropriately compensated as given in [2]. The integrative term of the i_τ regulator compensates the coupling of flux loop through k term. The back emf of motor linked via b term can be appropriately compensated by feed forward of back emf. The gain of current regulator are tuned by the same procedure as defined earlier,

$$k_{\mathrm{p},\tau} = \left(\frac{b}{L_{\mathrm{d}}}\right) \frac{1 + T_{\mathrm{s}}/3}{T_{\mathrm{c},\tau} + T_{\mathrm{s}}}$$

$$k_{\mathrm{i},\tau} = \left(\frac{b}{L_{\mathrm{d}}}\right) \frac{1 + T_{\mathrm{s}}/3}{4(T_{\mathrm{c},\tau} + T_{\mathrm{s}})}$$

The parameter $T_{\mathrm{c},\tau}$ is the closed loop time constant and the sole tuning parameter for the regulator. Since b is not constant, constant proportional gain will give different closed loop response at different flux situations [2]. In order to avoid a transient overcurrent, initially the regulator gains are calculated using variable b. As the control moves towards the MTPV region the magnetic parameter b and thus the gains will approach zero. This will result in loop instability. Therefore for a stable well damped response in the vicinity of the MTPV region, the gains are calculated using maximum value of b [11]. The maximum value or the constant $b_{\max}$ is determined from (4.7) using an unsaturated magnetic model of the machine.

4.5 Flux Observer

To accurately estimate the stator flux $\hat{\psi}_{\mathrm{s}}$ and angle $\hat{\delta}$, a reduced order closed loop flux observer proposed in [36] [37] is used (Figure 4.6). The flux estimation performed

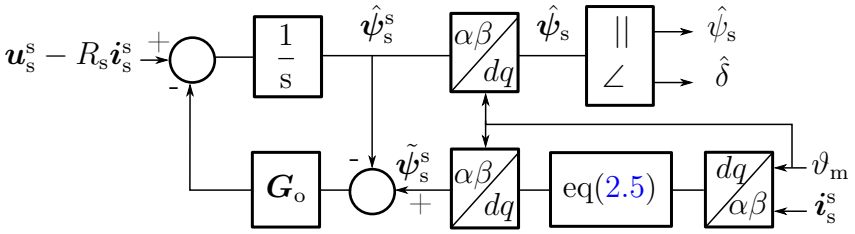

Figure 4.6: Flux observer scheme [36].

in stator coordinates is based on utilizing the motor magnetic model (2.5) below a certain frequency called the cross over frequency ω_o and by the voltage integration model above it. Since flux estimation is model dependent below ω_o, the outputs are susceptible to errors due to saturation effects, current ripple and other parameter uncertainties. Estimation by voltage measurement is highly noisy at speeds near zero speed. Therefore, the observer is structured in such a way that the estimation is performed by the magnetic model from zero speed to ω_o. The elements of the gain matrix $\boldsymbol{G}_\mathrm{o}$ set equal to ω_o determine the point of cross over between the two models [2, 3, 11]

$$\boldsymbol{G}_\mathrm{o} = \begin{bmatrix} \omega_\mathrm{o} & 0 \\ 0 & \omega_\mathrm{o} \end{bmatrix} \tag{4.14}$$

At high speeds the flux estimation is performed by voltage measurement which is more robust to parameter variation. Therefore, the goal is to estimate the flux which is derived as much as possible from the voltage measurement. The use of the constant magnetic model below ω_o deteriorates the control performance if it is improperly identified. If $\hat{\psi}_\mathrm{s}$ is under or overestimated the produced torque is higher or lower than the reference torque. Similarly, in case of error in $\hat{\delta}$, i_τ is not perfectly aligned with τ-axis which would also cause a reduction in the produced torque. However, even with a poor knowledge of the motor model, the current limit i_max is still respected.

4.6 MTPV Operation

It has been established in previous discussions that $b(\delta,\psi_\mathrm{s})$ affects the stability of τ-loop. For $b<0$ the affect of u_τ voltage component on torque regulation is reversed, i.e., the torque being produced could decrease instead of increasing as per commanded [11]. Therefore proper limitation of factor b, i.e., $b > 0$ is required to ensure τ-loop stability at all situations. Inspection of (4.8) reveals that $b = 0$ means derivative of the torque with respect to load angle is zero [11]. Thus, $b = 0$ trajectory is the MTPV limit in i_d-i_q plane (Figure 3.6(a)) [10]. The δ control loop is given in Figure 4.7.

The MTPV operation occurs at a specific value of δ called δ_max. The condition $\delta > \delta_\mathrm{max}$ would result in $b<0$ causing instability. Therefore, identification of δ_max is

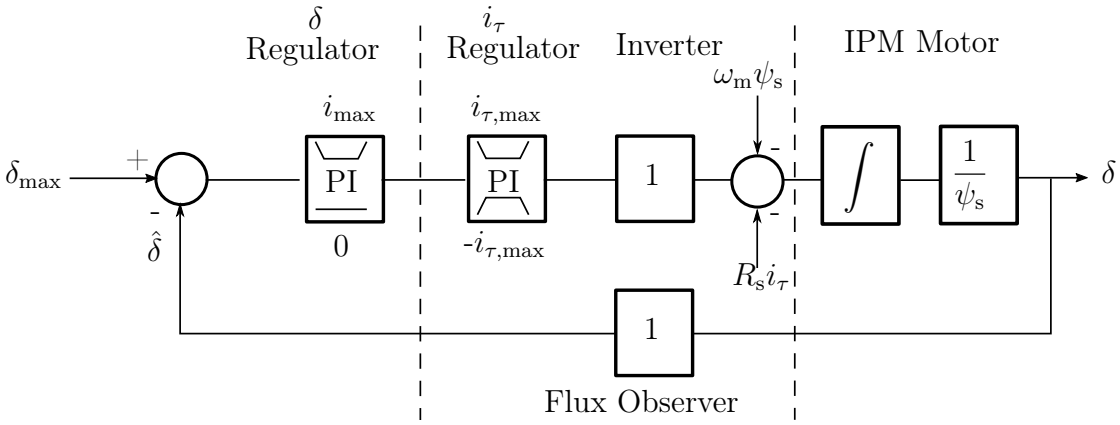

Figure 4.7: Dynamic block scheme representing δ_{max} regulation [3].

of utmost importance. The limitation δ_{max} can be obtained by posing the partial derivative of torque equation (4.3) with respect to the load angle δ equal to zero as,

$$\left(\frac{\partial T_e}{\partial \delta}\right)_{\psi_s=const} = 0 \tag{4.15}$$

from which we obtain the following solution

$$\delta_{max} = \cos^{-1}\left[\frac{\psi_{pm}L_q}{4\hat{\psi}_s(L_q - L_d)} - \sqrt{\left(\frac{\psi_{pm}L_q}{4\hat{\psi}_s(L_q - L_d)}\right)^2 + \frac{1}{2}}\right] \tag{4.16}$$

The resulting solution provides δ_{max} values for every motor type. The δ_{max} limitation for IPMs lies within the range $90° < \delta_{max} < 135°$. For IPMs with high saliency the value approaches 135° which is the theoretical δ_{max} limit for SyRMs. Conversely, for IPMs exhibiting magnetic characteristics similar to SPMs δ_{max} lies in the vicinity of 90° which is the δ_{max} limit for SPMs [3].

The MTPV operation is obtained by limitation of δ below δ_{max}. As mentioned earlier, there is a correspondence between the current component i_τ and δ. Limitation of δ produces a limitation of i_τ and vice versa. Operation on the MTPV trajectory is obtained by limiting the current reference $i_{\tau,ref}$ using the observed load angle $\hat{\delta}$ as shown in Figure 4.2. As we can observe from Figure 4.2, the MTPV limitation is performed by closed loop control of angle δ using a PI controller [3, 12, 13]. If the observed angle $\hat{\delta}$ becomes greater than the set point δ_{max} ($\hat{\delta} > \delta_{max}$), the PI controller generates a current component i_{MTPV}. This component is subtracted from the current limit i_{max} described in (4.11) to further reduce the maximum limit of $i_{\tau,ref}$. The reduction in magnitude of $i_{\tau,ref}$ by current component i_{MTPV} means that δ is exactly limited to δ_{max} by the regulator and b is also limited to 0 which corresponds to operation along the MTPV curve. It is to be noted that total limitation on $i_{\tau,ref}$ is determined by the sum of both the limitation due the inverter current limit i_{max} and the current component i_{MTPV} to keep motor operation stable in the MTPV region. The lower limit of the δ regulator is set to 0 which means that when

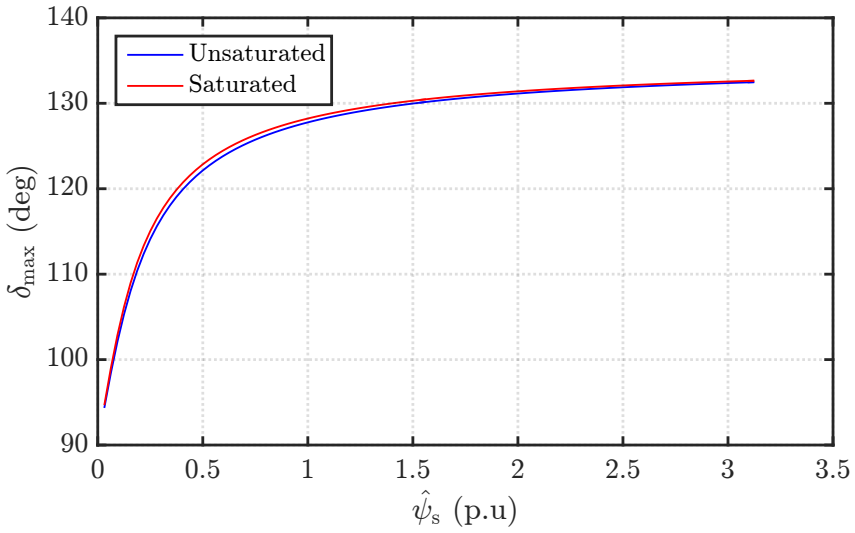

Figure 4.8: Effect of magnetic saturation on $\delta_{\max}$.

$\hat{\delta} < \delta_{\max}$, the regulator is off and $i_{\text{MTPV}} = 0$ (MTPV block is off). For stable design of the regulator, the upper limit is set to $i_{\max}$ to keep the output span as large as possible to keep $\delta_{\max}$ control stable even during worst case conditions, e.g., during transients [12].

The $\delta_{\max}$ equation (4.16) is highly model dependent because of L_{d}, L_{q} and ψ_{pm} terms. Simulations results have shown that the effect of saturation on $\delta_{\max}$ are quite negligible and if desired they can be ignored. Figure Figure 4.8 shows the variation of $\delta_{\max}$ limit against estimated flux $\hat{\psi}_{\text{s}}$ for a saturated and unsaturated case assuming constant rotor temperature. It can be inferred that saturation within the machine shifts the MTPV trajectory towards the horizontal d-axis. Even for the motor with moderately salient characteristics, the effect on $\delta_{\max}$ trajectory is quite minor and even if saturation is not taken into account in (4.16) a very good estimation of MTPV limit is possible. If in the case motor is poorly identified, $\delta_{\max}$ can be found by a series of no load acceleration test as pointed out in [12]. MTPV trajectory also varies with PM flux as it is dependent on the operating temperature of the motor. The increase in rotor temperature demagnetizes the magnets, thus reducing the flux and shifting the trajectory more towards the d-axis. For precise control during high speed operation, temperature effects should also be considered during $\delta_{\max}$ computation.

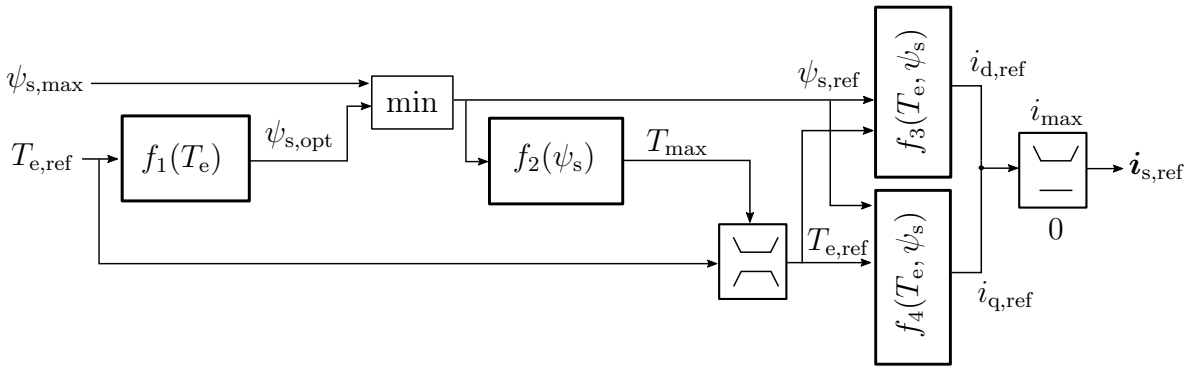

Figure 4.9: Reference generation scheme for LUT based approach [38].

4.7 Current Vector Control

To identify the performance of the DFVC technique it is compared with a conventional current vector control. The technique is reported in [38] and is based on optimal motor operation by exploiting actual experimental data. Figure 4.9 shows the block diagram for reference generation of the scheme. The controlled variables are the components i_d and i_q where the reference generation is based on the manipulation of flux magnitude ψ_s as in the case of the DFVC. The techniques makes use of the experimental measurements to construct LUTs for the MTPA and MTPV control. Since these tables are based on manipulation of actual motor magnetic maps the effect of saturation and cross saturation are inherently taken into account.

Similar to the DFVC approach the first 1-D LUT calculates the optimal flux reference to generate the requested torque on MTPA curve by procedure defined in 4.3.1. The optimal flux reference $\psi_{s,opt}$ is then compared with the maximum flux $\psi_{s,max}$ at a given speed to determine the region of operation, i.e., the FW or constant torque region. The MTPV control is achieved by direct limitation of the torque reference $T_{e,ref}$ through T_{max} by a second 1-D LUT. The procedure for construction of the MTPV LUT is given in Figure 4.10. The variables $\psi_{s,ref}$ and $T_{e,ref}$ are then used to determine current set points $i_{d,ref}$ and $i_{q,ref}$ by two additional 2-D LUTs (f_3,f_4). The current references are then limited to respect the i_{max} limit. It should be noted that current limitation in [38] is taken into account in LUT $f_2(\psi_s)$. However, in this scenario the current is limited explicitly by a limitation block. The approach is simpler, requiring less manipulation of data.

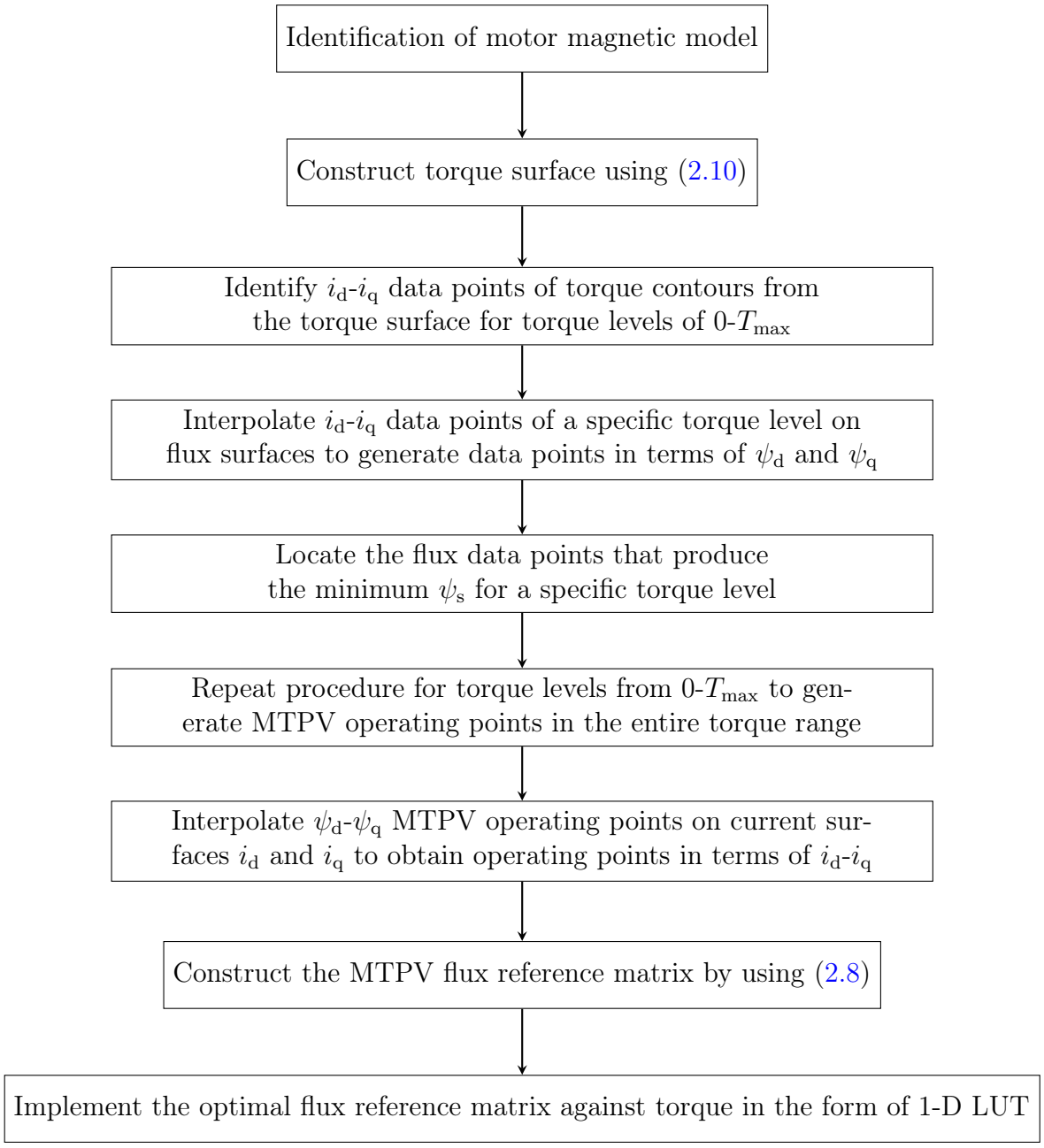

Figure 4.10: Flow diagram of maximum torque calculation process in the MTPV region.

5 Results

The results of this thesis are divided into five cases. In case 1, the DFVC scheme is simulated considering a linear magnetic model of the motor. In case 2, the robustness of vector control technique is analysed against parameter variation by a series of load test. The robustness is further analysed and time-domain behaviour of the motor is simulated introducing a saturation model in the plant in case 3. Saturation model is then introduced both in the plant and in the controller. The results are documented as case 4. In case 5, a benchmark current vector control scheme is compared with the DFVC in order to determine the optimality in terms of performance. The simulations are performed in MATLAB/Simulink environment. Simulations are performed using the data of a 7.5 kW IPM whose ratings are given in Table 5.1.

Case 1: Linear magnetic model in the plant and in the controller.
Case 2: Robustness analysis of DFVC scheme against parameter variation.
Case 3: Robustness analysis by implementing saturation model in plant with linear magnetic model in the controller.
Case 4: Consideration of saturation both in plant and in the controller.
Case 5: Comparison of the DFVC and current vector control approach.

Simulation Results

Parameters of the simulated motor are shown in Table 5.2. The plant model is implemented in continuous-time domain while the DFVC and flux observer are implemented in discrete-time domain. The discretization is attained using the Forward Euler method. The current as well as rotor speed are obtained as the output of the PMSM block. Synchronous sampling is implemented and all simulations are performed at the sampling frequency of $f_s = 10$ kHz.

Table 5.1: Ratings of the IPM

Rated power	P_{N}	7.5 kW
Rated voltage (L-L rms)	U_{N}	246 V
Rated current (rms)	I_{N}	17.6 A
Rated torque	T_{N}	24 Nm
Rated frequency	f_{N}	100 Hz
Rated speed	ω_{N}	3000 r/min
Pole pairs	p	2

Table 5.2: Parameters of the simulated IPM

Nominal d-axis inductance	L_{d}	3.3 mH
Nominal q-axis inductance	L_{q}	31.2 mH
PM flux	ψ_{pm}	0.116 Wb
Stator resistance	R_{s}	0.22 Ω
Moment of inertia	J	0.005 kgm^2

5.1 Case 1

In this case, the response of DFVC scheme is studied in linear magnetic operating conditions. Saturation and cross saturation in the plant as well as in the controller is neglected. The simulations are conducted in the speed control mode by applying a speed step of $\omega_{\mathrm{m,ref}} = 4$ p.u. The maximum torque T_{max} is limited to 1.5 times the rated torque, i.e., $T_{\mathrm{max}} = 1.5\ T_{\mathrm{N}}$. Such a selection allows to observe the operating capabilities of the motor in all regions of operation, i.e., MTPA and FW including the MTPV. The MTPA operating point is determined from a 16 point LUT based on speed controller output $T_{\mathrm{e,ref}}$.

In order to observe the performance of the flux observer on DFVC scheme, the results of this section are divided into two subsections. In the first scenario, vector control is implemented by assuming actual flux feedback information from the plant model. The second case is based on estimating the stator flux through the flux observer. Both the tests are conducted at the same test conditions.

5.1.1 Ideal flux feedback

A speed step is applied at $t = 0.2$ s and the motor is accelerated by T_{max}. The operating points on the MTPA curve for T_{max} request are determined through the

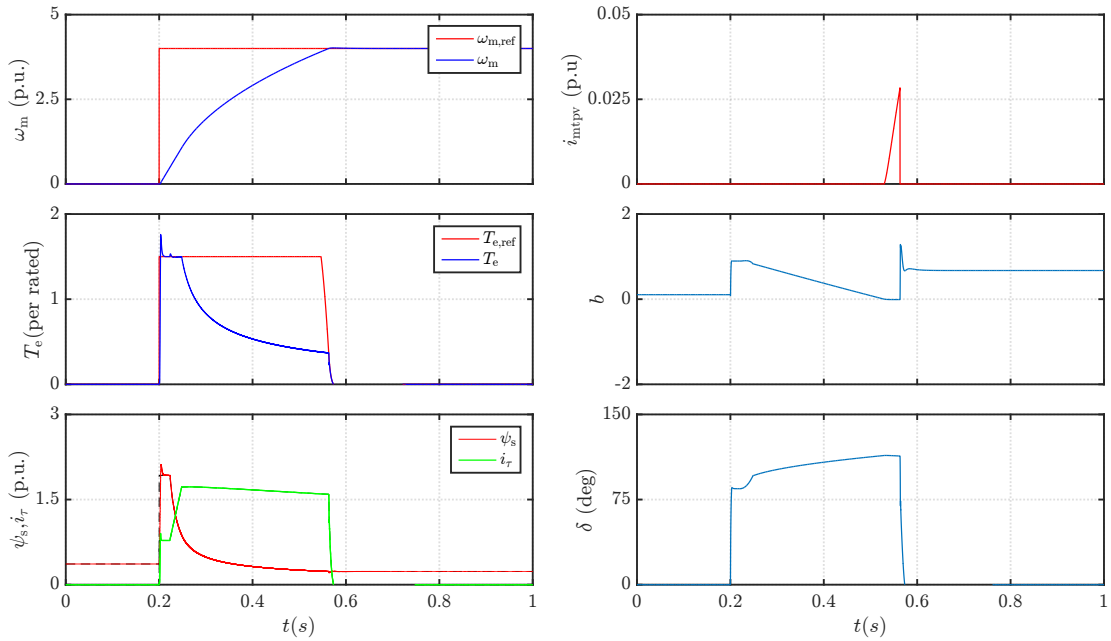

(a) (b)

Figure 5.1: Simulations results of speed step $\omega_{m,ref} = 4$ p.u. for case 1 with actual flux feedback in time-domain (a) The uppermost subplot shows the actual and reference speed, the second subplot shows the actual and reference torque, the third subplot shows the state variables (b) The first subplot shows the current i_{MTPV}, the second subplot shows the variable b, the third subplot shows the load angle δ.

LUT as depicted in Figure 5.2. The motor is accelerated by T_{max} till terminal voltage of the motor is saturated by the available u_{dc} at $t = 0.22$ s. This indicates the onset of FW and is followed by the reduction of stator flux through the FW algorithm as shown in Figure 5.1. The decrease in ψ_s is accompanied by an increase in the current i_τ so that the torque remains constant. The maximum torque solution is now found by moving along the constant torque curve as the speed increases from $\omega_m = 0.4$ p.u. to 1.0 p.u. during the time interval $t = 0.22$-0.24 s. From $\omega_m = 1.0$ p.u. to 3.2 p.u., the torque should be reduced because of the current limit otherwise no optimal solution is found. The increase of ω_m in the FW region is accompanied by an increase in the load angle δ as shown in Figure 5.1. Angle δ approaches its maximum limit $\delta_{max} \approx 113°$ at $t = 0.52$ s which implies that the reference speed should now be pursued by operation on the MTPV curve. The MTPV operation is implemented by generation of current component i_{MTPV} by limitation of angle δ to δ_{max} within time interval $t = 0.52$-0.56 s. As pointed out in section 4, the variable b is accurately limited to zero by the δ loop control during the MTPV operation. The motor speed reaches its reference at $t = 0.56$ s.

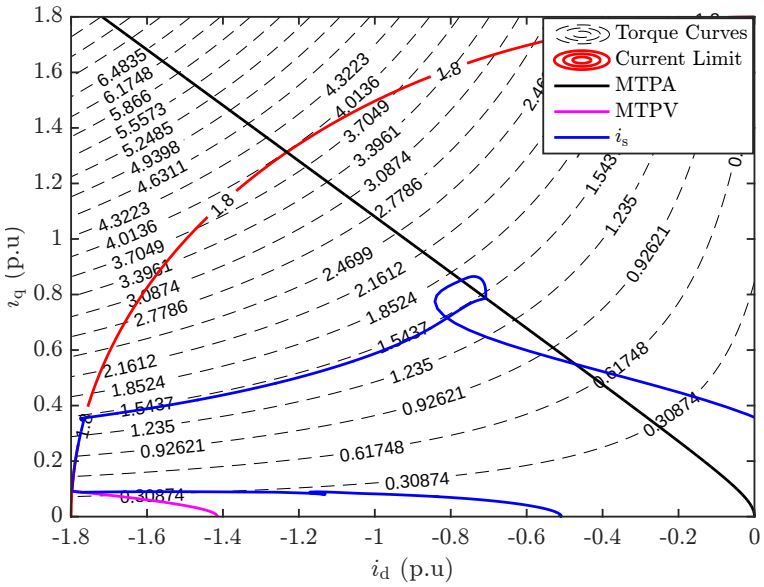

Figure 5.2: Simulations results of speed step $\omega_{m,ref} = 4$ p.u. for case 1 with actual flux feedback in the i_d-i_q domain.

5.1.2 Flux estimation through the flux observer

The control performance of the DFVC scheme largely depends on the accuracy of the flux observer. The observer cross over frequency that separates two modes of estimation is set at 40 Hz. The speed step of $\omega_{m,ref} = 4$ p.u. is applied at $t = 0.2$ s. Errors in discretization lead to underestimation of the flux by the observer. The produced torque is thus higher than the reference as shown in Figure 5.3. Since $\hat{\delta}$ is also determined by the flux observer, any error in the estimation of flux translates to errors in $\hat{\delta}$ estimation. Errors in $\hat{\delta}$ means that the controlled i_τ is not perfectly orthogonal to controlled motor flux ψ_s. This will also result in inaccuracies in the produced torque. Because of high torque, the motor is accelerated faster and the FW is triggered at $t = 0.22$ s. The current limit is reached at time instant $t = 0.24$ s and further increase in speed calls for reducing the produced torque as shown in Figure 5.3. In the FW region, $\hat{\delta}$ is overestimated at every time instant compared to the former case. As a result, the limitation of $\hat{\delta}$ by δ_{max} is triggered earlier at time instant $t = 0.38$ s compared to $t = 0.52$ s which was the limitation time instant in the former case. This can be understood from Figure 5.4 where the actual current $\boldsymbol{i}_s$ is limited before the actual MTPV trajectory is reached. Speed reaches its reference at $t = 0.56$ s. Inaccuracies in the flux estimation is a result of discretization errors and due to the inaccurate magnetic model identification in the observer. Since a linear magnetic model is being used, the parameters $\hat{L}_d$ and $\hat{L}_q$ are exactly identified. Therefore, the second option should be eliminated. Ultimately, the inaccuracies are a result of the first option. We can see here that the Forward Euler method chosen to discretize the continuous-time observer in stator coordinates provides marginally good results.

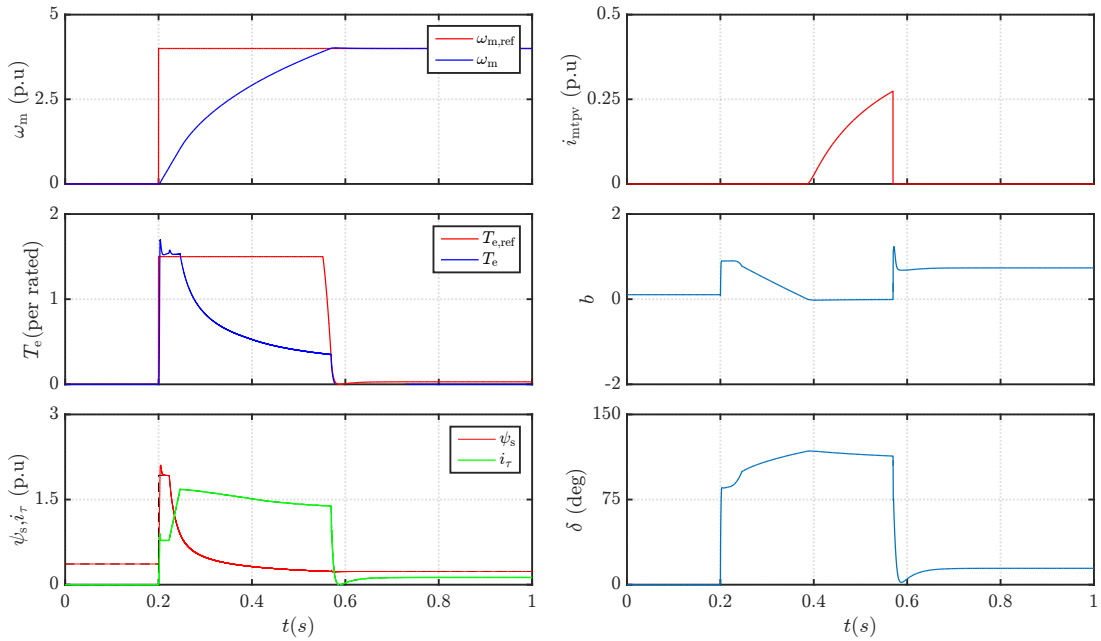

Figure 5.3: Simulations results of speed step $\omega_{m,ref} = 4$ p.u. for case 1 with flux observer in time-domain (a) The uppermost subplot shows the actual and reference speed, the second subplot shows the actual and reference torque, the third subplot shows the state variables (b) The first subplot shows the current i_{MTPV}, the second subplot shows the variable b, the third subplot shows the load angle δ.

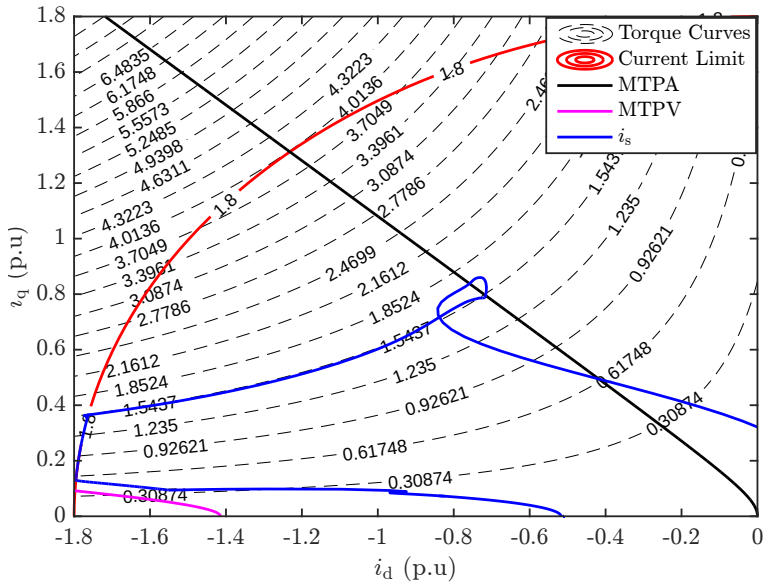

Figure 5.4: Simulations results of speed step $\omega_{m,ref} = 4$ p.u. for case 1 with flux observer in the i_d-i_q domain.

Table 5.3: Models describing the variation of parameter under test

Model	Variation in %
Model 1	Rated
Model 2	-50% of Rated
Model 3	+50% of Rated

Even though the produced torque is slightly higher than the reference, the current $\boldsymbol{i}_\mathrm{s}$ is accurate to what it should be as dictated by the MTPA control. Additionally, the inverter current limit is respected in all modes of operation.

5.2 Case 2

The robustness of the DFVC scheme is analysed by introducing erroneous parameters in the controller. Robustness is tested from a series of load tests conducted at low speed. Tests are performed in the torque control mode ín which the motor is operated at a specific speed as the load is varied. Robustness of the controller against variation in $\hat{L}_\mathrm{d}$, $\hat{L}_\mathrm{q}$ and $\hat{\psi}_\mathrm{pm}$ is studied individually. It is to be noted that the parameters in the plant are equal to their rated values. Simulations have shown that the control is quite insensitive to variation in resistance R_s therefore the results are not documented. The linear magnetic model of the machine is used both in the plant and the controller. A specific motor parameter under study is varied according to Table 5.3. Model 1 describes that the estimated parameter in the controller is equal to its rated value. Therefore, it is the best case condition as the estimated parameters are identified exactly as in the plant. Model 2 deals with the condition when the parameter under test is less than 50% of its rated value while all the other parameters are equal to the rated. Similarly, model 3 deals with overestimation of parameter and is self explanatory. Variation of parameters is also considered in the flux observer. As discussed earlier, the flux observer is based on estimating flux using the current-flux model below the cross over frequency ω_o while the voltage model above it. The current model is more susceptible to deterioration in performance if the magnetic model is imprecise than the voltage model. Therefore, the tests are conducted at speeds below ω_o to include observer effects. The motor is operated at a speed of $\omega_\mathrm{m} = 0.15$ p.u. corresponding to the motor frequency of 16 Hz which is well below the observer cross over frequency of 40 Hz. Load of the motor is ramped up from 0-1.5T_N. Motor parameters are then varied individually according to Table 5.3.

Table 5.4: Variation in $\hat{L}_\mathrm{d}$: Conditions required to produce $T_\mathrm{e} = 1.5T_\mathrm{N}$

	T_e	i_s	ψ_s	Remarks
Model 1	$1.5T_\mathrm{N}$	$1.4i_\mathrm{N}$	$2.07\psi_\mathrm{N}$	Optimal
Model 2	$1.5T_\mathrm{N}$	$\approx 1.4i_\mathrm{N}$	$\approx 2.07\psi_\mathrm{N}$	$\hat{\psi}_\mathrm{s} < \psi_\mathrm{s}$
Model 3	$1.5T_\mathrm{N}$	$\approx 1.4i_\mathrm{N}$	$\approx 2.07\psi_\mathrm{N}$	$\hat{\psi}_\mathrm{s} > \psi_\mathrm{s}$

5.2.1 Variation in $\hat{L}_\mathrm{d}$

The effects of variation in $\hat{L}_\mathrm{d}$ is reported in Table 5.4 that state the current and flux requirements to produce maximum load torque in every model. The torque factor k_t (Nm/A) represents the most optimal torque to current ratio that the motor can produce under the voltage limit. Optimal k_t is determined by experimental data shown in Figure 5.5 along with torque factors resulting from other cases. If a particular k_t trajectory lies below the optimal, more stator current will be required to produce a certain torque and vice versa. The trajectory of stator current vectors in the i_d-i_q domain is also shown in Figure 5.5.

For the ideal case, i.e., model 1 i_s follows the MTPA curve exactly while the torque factor reproduces the optimal trajectory. The load torque under consideration, i.e., T_e=$1.5T_\mathrm{N}$ is produced by the stator current and flux as shown in Table 5.4. The results of this case have already been studied in former sections. Model 2 deals with the behaviour of the control system if $\hat{L}_\mathrm{d}$ is underestimated. The imprecise magnetic model in the flux observer results in $\hat{\psi}_\mathrm{s}$ being under estimated. The actual flux in the machine is higher than the one estimated by the observer. Referring to Table 5.4 even if the actual stator flux is higher in the plant, it is approximately equal to what it was in the case of model 1. Thus, the stator current required to produce the load torque is also the same. The control response is similar for model 3 where $\hat{L}_\mathrm{d}$ is overestimated. The main difference being that $\hat{\psi}_\mathrm{s}$ is now overestimated by the observer. The stator flux and current are approximately the same as in the case of model 1 for all loads. From Figure 5.5, we can see that for all models the trajectory of the stator current nearly follow the MTPA curve during entire loading operation. Furthermore, the trajectory of torque factors is equal to optimal for all cases. We can infer that the deviation in $\hat{L}_\mathrm{d}$ has a negligible effect on control performance under ω_o.

5.2.2 Variation in $\hat{L}_\mathrm{q}$

The effects of variation in $\hat{L}_\mathrm{q}$ are similar to variation in $\hat{L}_\mathrm{d}$ but more prominent. The trajectory of the stator current vector and torque factor k_t is reported in Figure 5.6. In model 2, the estimated stator flux is underestimated. The actual flux required to produce concerned torque is lower than in model 1 as shown in Table 5.5. The

Table 5.5: Variation in $\hat{L}_q$: Condition required to produce $T_e = 1.5T_N$

	T_e	i_s	ψ_s	Remarks
Model 1	$1.5T_N$	$1.4i_N$	$2.07\psi_N$	Optimal
Model 2	$1.5T_N$	$1.42i_N$	$1.75\psi_N$	$\hat{\psi}_s < \psi_s$
Model 3	$1.5T_N$	$1.41i_N$	$2.17\psi_N$	$\hat{\psi}_s > \psi_s$

Table 5.6: Variation in $\hat{\psi}_{pm}$: Condition required to produce $T_e = 1.5T_N$

	T_e	i_s	ψ_s	Remarks
Model 1	$1.5T_N$	$1.4i_N$	$2.07\psi_N$	Optimal
Model 2	$1.5T_N$	$\approx 1.4i_N$	$1.98\psi_N$	$\hat{\psi}_s > \psi_s$
Model 3	$1.5T_N$	$\approx 1.4i_N$	$2.1\psi_N$	$\hat{\psi}_s < \psi_s$

reduced stator flux is compensated by a higher stator current thus the losses are increased. The effect becomes more evident at high loads as the stator current trajectory diverges from the MTPA trajectory. The fact is further confirmed as the k_t trajectory follows the optimal trajectory for a limited load region and diverges from it as the loading is increased as shown in Figure 5.6. In model 3, $\hat{\psi}_s$ is over estimated for the entire loading region. In order to produce the same torque, a higher stator current and flux is required in comparison with case 1. It is evident that $\hat{L}_q$ term has a considerable effect on control performance below ω_o of the observer. Observer error in case of variation in $\hat{L}_q$ is substantial in comparison with the variation in $\hat{L}_d$. Higher stator current is required regardless if $\hat{L}_q$ is under or overestimated. The effect becomes prominent particularly as the load is increased.

5.2.3 Variation in $\hat{\psi}_{pm}$

Trajectory of the stator current vector and torque factor k_t is shown in Figure 5.7. In case of model 2, $\hat{\psi}_s$ is initially underestimated for low loads. However, as the loading is increased it is overestimated. The trajectory of k_t follows the optimal trajectory. Hence the stator current required to produce particular torque is approximately the same as in model 1. However, the flux required to produce the load torque is less than the model 1 as it can be seen in Table 5.6. In case of model 3, $\hat{\psi}_s$ is initially overestimated for low loads but then it is underestimated as the loading is increased. The behaviour is exactly reverse of model 2. To produce the maximum torque, the current requirement is the same as in model 1 but at a higher flux than the optimal as shown in Table 5.6. This fact is also confirmed through the trajectory of torque factor k_t in Figure 5.7 that lies on the optimal trajectory for high loads.

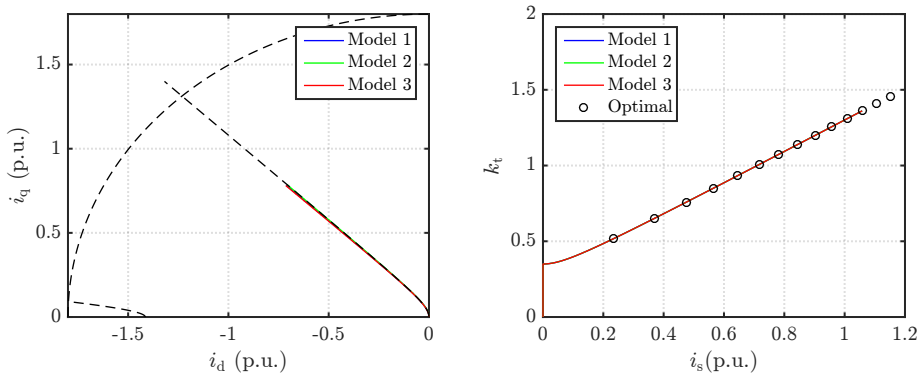

Figure 5.5: Results for variation in $\hat{L}_d$. The subplot on left shows the trajectory of stator current in i_d-i_q domain and subplot on right shows the torque factor against stator current.

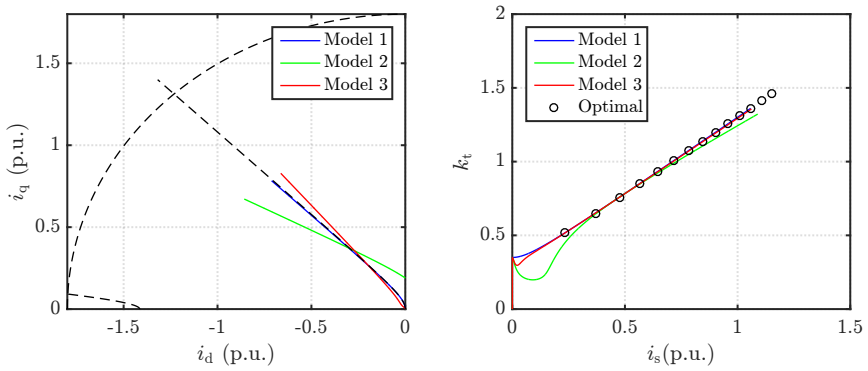

Figure 5.6: Results for variation in $\hat{L}_q$. The subplot on left shows the trajectory of stator current in i_d-i_q domain and subplot on right shows the torque factor against stator current.

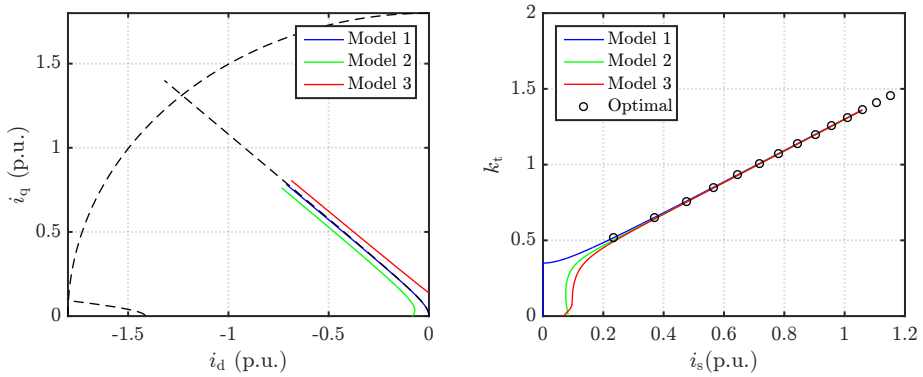

Figure 5.7: Results for variation in $\hat{\psi}_{pm}$. The subplot on left shows the trajectory of stator current in i_d-i_q domain and subplot on right shows the torque factor against stator current.

Table 5.7: Fitted parameters for IPM

L_{du}	L_{qu}	a_{dd}	a_{dq}	a_{qq}	S	T	U	V	i_{F}
0.0033	0.0312	0	0	2081.6	0	5	0	0	35.36

It can be inferred from the results that variation of $\hat{\psi}_{\mathrm{pm}}$ has a noticeable impact on flux estimation below ω_{o} however the stator current requirement for cases 2 and 3 is approximately the same for all loads. We can infer that the DFVC control is most susceptible to variation in $\hat{L}_{\mathrm{q}}$ and $\hat{\psi}_{\mathrm{pm}}$ as a result of errors in flux estimation and in reference generation. Control is least susceptible to variation in $\hat{L}_{\mathrm{d}}$ particularly because of its minor contribution to the stator flux generation.

5.3 Saturation

In order to achieve high torque requirements and better control performance, saturation of flux ψ_{d} and ψ_{q} must be considered in both the plant and the controller. In this study, saturation is modelled by considering currents i_{d},i_{q} as a function of fluxes ψ_{d} and ψ_{q}. The actual currents i_{d} and i_{q} are determined at every sampling instant using explicit functions proposed in [21]. The model is modified to take into account the effect of PM flux in IPMs,

$$i_{\mathrm{d}}(\psi_{\mathrm{d}},\psi_{\mathrm{q}}) = \psi_{\mathrm{d}}\left[\frac{1}{L_{\mathrm{du}}} + a_{\mathrm{dd}}|\psi_{\mathrm{d}}|^{S} + \frac{a_{\mathrm{dq}}}{V+2}|\psi_{\mathrm{d}}|^{U}|\psi_{\mathrm{q}}|^{V+2}\right] - i_{\mathrm{F}} \tag{5.1a}$$

$$i_{\mathrm{q}}(\psi_{\mathrm{d}},\psi_{\mathrm{q}}) = \psi_{\mathrm{q}}\left[\frac{1}{L_{\mathrm{qu}}} + a_{\mathrm{qq}}|\psi_{\mathrm{q}}|^{T} + \frac{a_{\mathrm{dq}}}{U+2}|\psi_{\mathrm{d}}|^{U+2}|\psi_{\mathrm{q}}|^{V}\right] \tag{5.1b}$$

where L_{du} and L_{qu} are the unsaturated inductances and a_{dd}, a_{dq}, a_{qq}, S, T, U, V, i_{F} are non-negative constants. The estimated flux $\hat{\psi}_{\mathrm{d}}$ and $\hat{\psi}_{\mathrm{q}}$ were calculated from the experimental data in rotor coordinates using the functions,

$$\hat{\psi}_{\mathrm{d}} = \frac{u_{\mathrm{q}} - R_{\mathrm{s}} i_{\mathrm{q}}}{\omega_{\mathrm{m}}} \tag{5.2a}$$

$$\hat{\psi}_{\mathrm{q}} = -\frac{u_{\mathrm{d}} - R_{\mathrm{s}} i_{\mathrm{d}}}{\omega_{\mathrm{m}}} \tag{5.2b}$$

Experimental data can be gathered by, e.g., the procedure defined in [34]. Calculated experimental data is then fitted to explicit functions to obtain the fitting parameters. Fitted parameters for the motor under test are reported in Table 5.7 while the experimental data and the fitted curve are shown in Figure 5.8. It can be seen that curves from the model fit the experimental data quite well. Experimental data shows that the motor suffers from minor cross saturation at high currents.

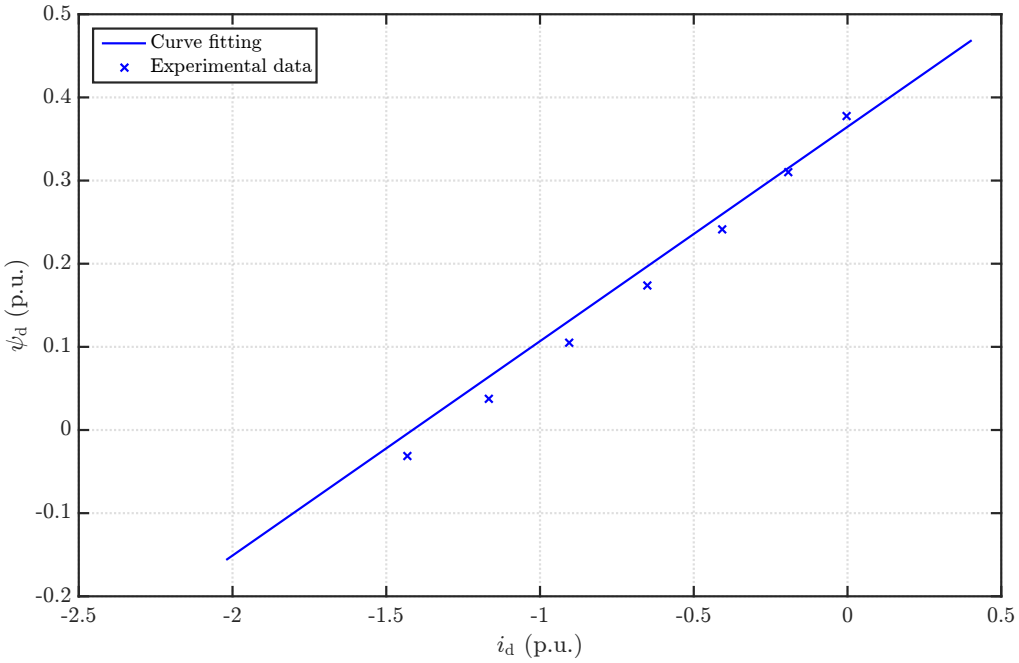

(a)

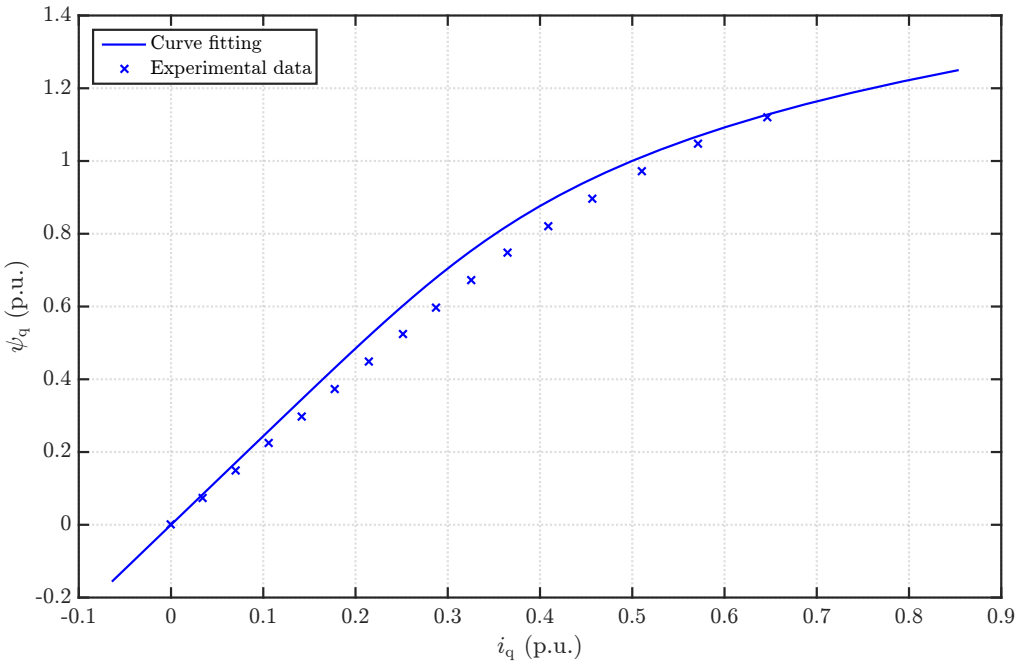

(b)

Figure 5.8: Results from curve fitting and experimental data (a) i_d as a function of ψ_d for $\psi_q = 0$ p.u.; (b) i_q as a function of ψ_q for $\psi_d = 0$ p.u.. The fluxes at rated operating point are : $\psi_d = 0.09$ p.u.,$\psi_q = 0.92$ p.u.

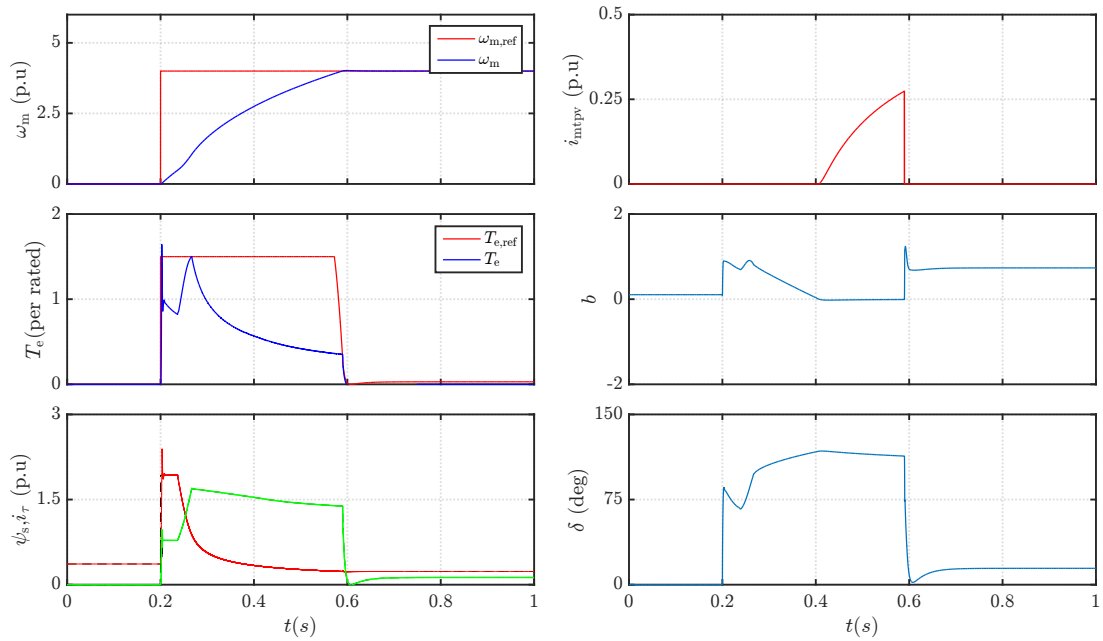

(a) (b)

Figure 5.9: Simulations results of speed step $\omega_{m,ref} = 4$ p.u. for case 3 in time-domain (a) The uppermost subplot shows the actual and reference speed, the second subplot shows the actual and reference torque, the third subplot shows the state variables (b) The first subplot shows the current i_{MTPV}, the second subplot shows the variable b, the third subplot shows the load angle δ.

5.4 Case 3

In this case, the performance and robustness of the DFVC scheme is examined by taking into account saturation in the plant but not in the controller. Figure 5.9 shows the response of the motor to a speed step input of $\omega_{m,ref} = 4$ p.u. given at $t = 0.2$ s. Inconsideration of saturation in MTPA LUT results in inaccurate references to the controller. As a result, the torque is lower than its reference. Furthermore, the variations of inductances in the plant result in a peak in stator current that violates i_{max} limit as shown in Figure 5.10. Within the constant torque region the operating points are far from the one determined by the saturated MTPA curve. At time instant $t = 0.23$ s, the voltage limit saturates and the FW is activated as flux begins to decrease. The rise in produced torque during $t = 0.24$-0.26 s (Figure 5.9) is because the operating points are selected on increasing torque curves as the reference flux is reduced. The current limit is approached at a speed of $\omega_m = 1.05$ p.u. during time instant $t = 0.26$ s, indicating operating points should now be selected on i_{max} circle as shown in Figure 5.10. Beyond instant $t = 0.26$ s, the behaviour of drive is similar to case 1 with estimation being performed by the flux observer. Angle $\hat{\delta}$ is overestimated, thus limitation by δ_{max} triggers the MTPV operation before the actual limit is reached. The MTPV operation is depicted by generation of current

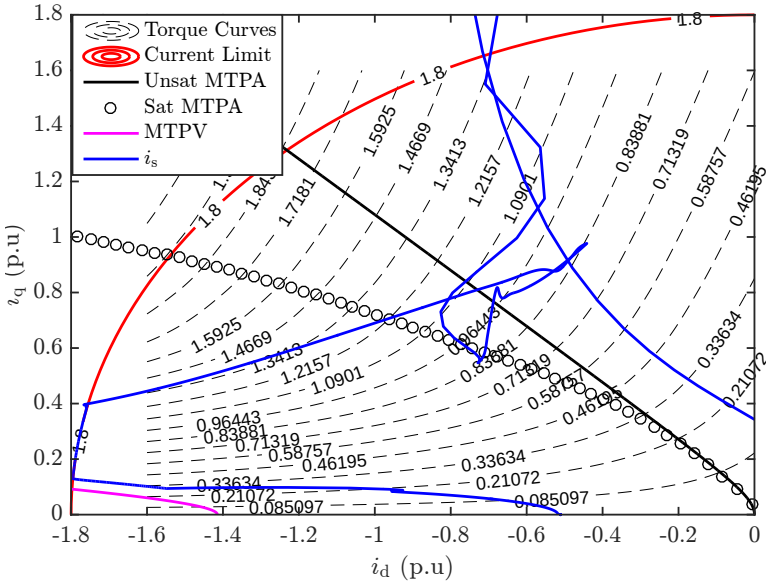

Figure 5.10: Simulations results of speed step $\omega_{m,ref} = 4$ p.u. for case 3 in the i_d-i_q domain.

i_{MTPV} during time instant $t = 0.4$-0.58 s. As it can be seen, the control behaviour is unsatisfactory in the constant torque mode which points to the fact that saturation effects should be taken into account in the controller for accurate torque production. Despite such poor performance, the DFVC follows the MTPV limits well in the FW region.

5.5 Case 4

Saturation is now implemented both in the plant and in the controller. Since estimation of flux is highly dependent on the motor magnetic model below ω_o, therefore saturated values of L_d and L_q must be used in the observer as well. Saturation in the controller is taken into account using 2-D LUTs. The MTPA LUT is determined by the procedure defined in section 4. Speed step of $\omega_{m,ref} = 4$ p.u. is applied at $t = 0.2$ s as shown in Figure 5.11. Since the MTPA LUT is built through manipulation of actual motor experimental data, saturation and cross saturation within the plant are inherently taken into account. The resulting references ψ_s and i_τ accurately produce the maximum torque as shown in Figure 5.11. In the constant torque region, the motor is accelerated within the interval $\omega_m = 0$-0.7 p.u. by the operating points lying on saturated MTPA curve. The stator current required to produce the requested torque during saturation is approximately 1.4 times the unsaturated case. The FW is triggered at $t = 0.23$ s and operating points are selected along the maximum torque curve. Ideally, the torque should remain constant but errors in flux estimation increases the produced torque. The current limit is approached at $t = 0.24$ s and operating points are selected on the i_{max} circle as speed increases to $\omega_m = 2.8$ p.u..

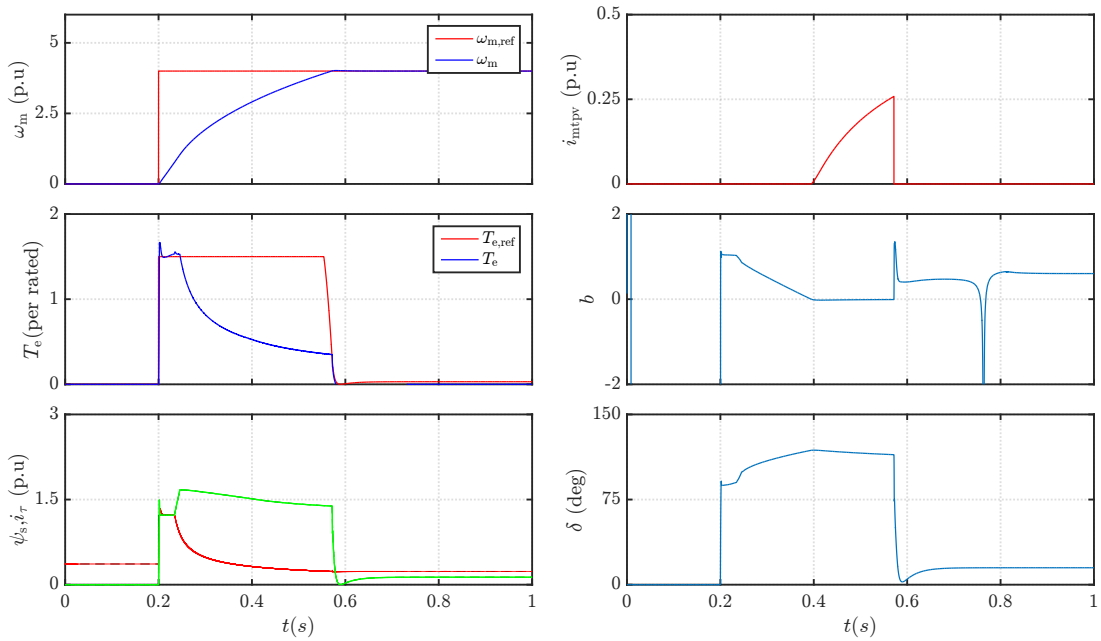

(a) (b)

Figure 5.11: Simulations results of speed step $\omega_{m,ref} = 4$ p.u. for case 4 in time-domain (a) The uppermost subplot shows the actual and reference speed, the second subplot shows the actual and reference torque, the third subplot shows the state variables (b) The first subplot shows the current i_{MTPV}, the second subplot shows the variable b, the third subplot shows the load angle δ.

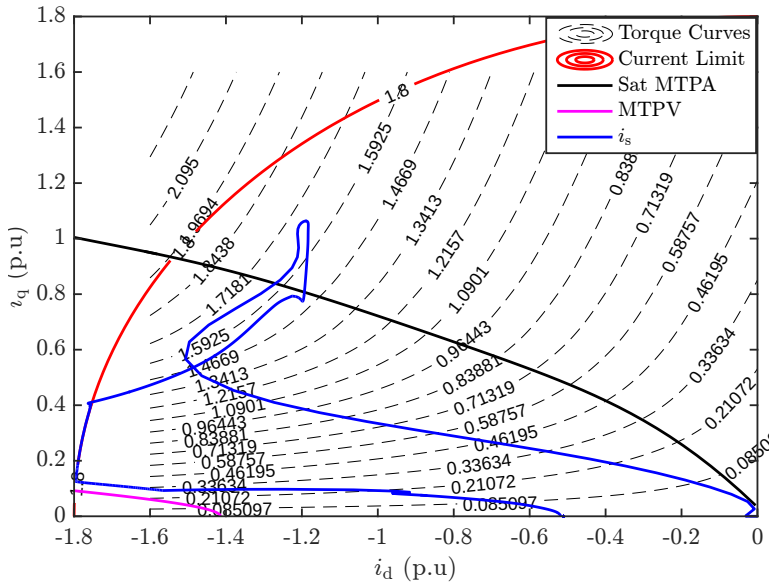

Figure 5.12: Simulations results of speed step $\omega_{m,ref} = 4$ p.u. for case 4 in the i_d-i_q domain.

The machine enters the MTPV region beyond time interval $t = 0.4$ s as $\hat{\delta}$ grows larger than $\delta_{\max}$. Similar to previous cases, error in discretization causes the control system to trigger i_{MTPV} current even before the actual limit is reached. The motor speed achieves its reference at $t = 0.57$ s. As defined in section 4, saturation phenomenon has negligible impact on the MTPV trajectory.

5.6 Case 5

To determine the optimality in terms of performance, the DFVC is compared with a current control approach implemented in the rotor reference frame. The technique is defined in section 4. Results of simulation for a speed step of $\omega_{\text{m,ref}} = 5$ p.u. are shown in Figure 5.13. A larger speed step results in the drive operating on the MTPV trajectory for an extended period of time. This helps in better comparison between the two techniques in the high speed region. In order to produce the requested torque, MTPA LUT generates the flux reference within time interval $t =$ 0.2-0.23 s during which the speed rises to 0.8 p.u.. The flux weakening is activated beyond $t = 0.23$ s. The torque should remain constant for $t = 0.23$-0.25 s as the drive operates on the constant torque curve of $T_{\text{e}} = 1.5T_{\text{N}}$. Current limit is reached at $t = 0.25$ s. The drive operates on the current limit for $t = 0.25$-0.53 s as speed is further increased from $\omega_{\text{m}} = 1.4$-3.7 p.u.. As a result of explicit current limitation, the torque response is not smooth in this region and the actual flux is lower than the reference. Beyond $t = 0.53$ s, the high speed operation is dictated by operation on the MTPV trajectory. The reference torque is limited to $T_{\max}$ by the second 1-D LUT as shown in Figure 4.9. The speed reaches its reference at $t = 0.77$ s. The response of current vector control for the speed step in i_{d}-i_{q} domain is shown in Figure 5.14.

Figure 5.15 shows the response of the drive using the two control strategies when subjected to speed input of $\omega_{\text{m,ref}} = 5$ p.u.. The figures depict the transition of the stator current and flux as the operating points move from the MTPA to the MTPV curve. The DFVC response is recorded by utilizing the flux information from the observer indicated by blue line and by assuming ideal flux information from the plant indicated by the red line. The operating condition of the drive on the MTPA curve is indicated by a red dot in Figure 5.15. Since the current vector control is the benchmarked technique so the limits for the region of operation are drawn by its results. In the constant torque region the DFVC has a higher torque factor for a given current than the current control approach. Within the current limited region, the results for both cases of the DFVC are identical. From Figure 5.15 we can see that the current limit for the benchmark technique is met at a delayed interval. The response to the DFVC scheme with ideal flux feedback and the LUT based approach in the MTPV region are the same. Since the MTPV limit is triggered earlier in the case of DFVC (with the flux observer), the torque per flux is reduced.

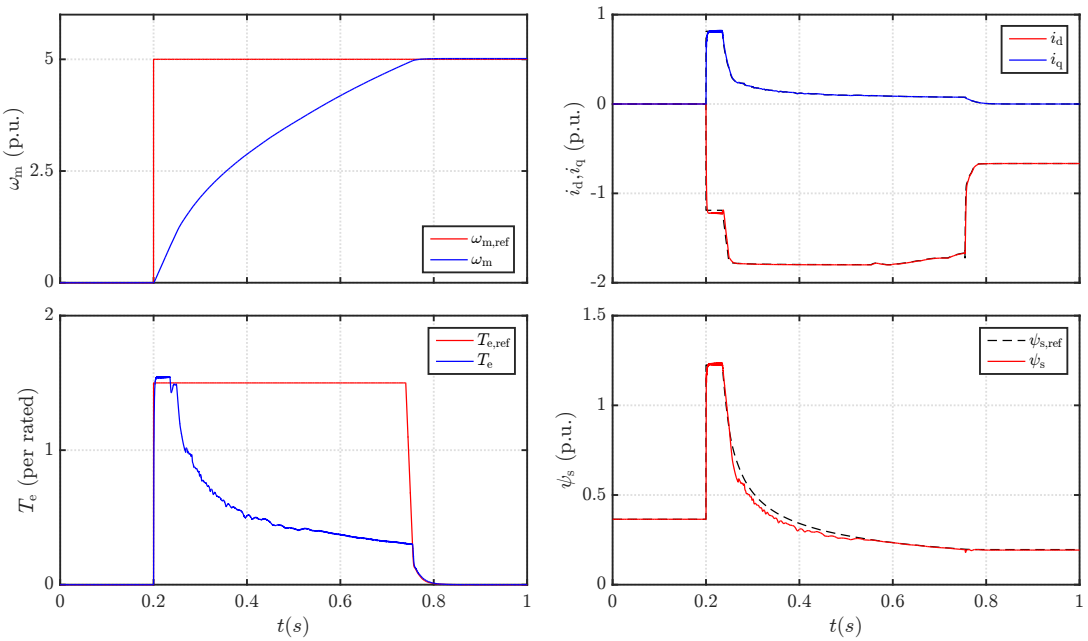

(a) (b)

Figure 5.13: Simulations results of speed step $\omega_{m,ref} = 5$ p.u. for current vector control scheme in time-domain (a) The uppermost subplot shows the actual and reference speed, the second subplot shows the actual and reference torque (b) The first subplot shows the current references and actual currents, the second subplot shows the stator flux.

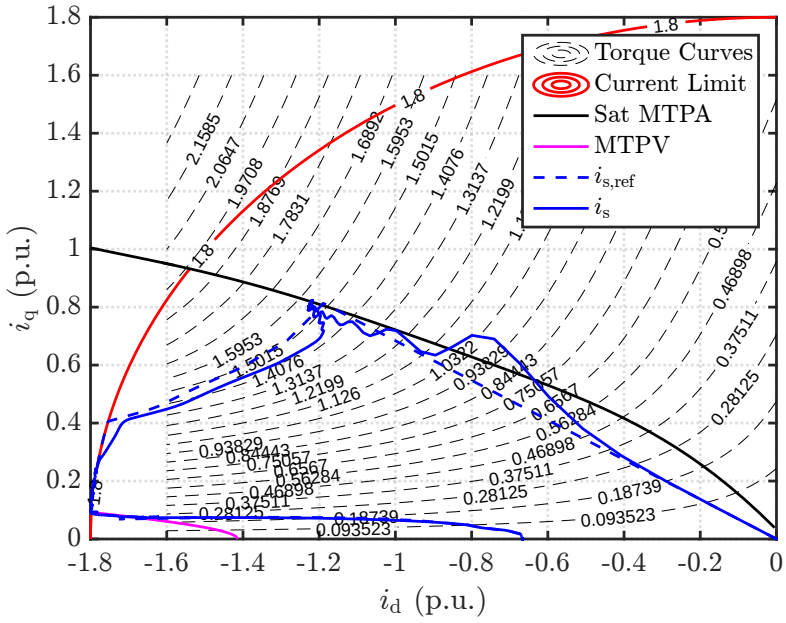

Figure 5.14: Simulations results of speed step $\omega_{m,ref} = 5$ p.u. for current vector control scheme in the i_d-i_q domain.

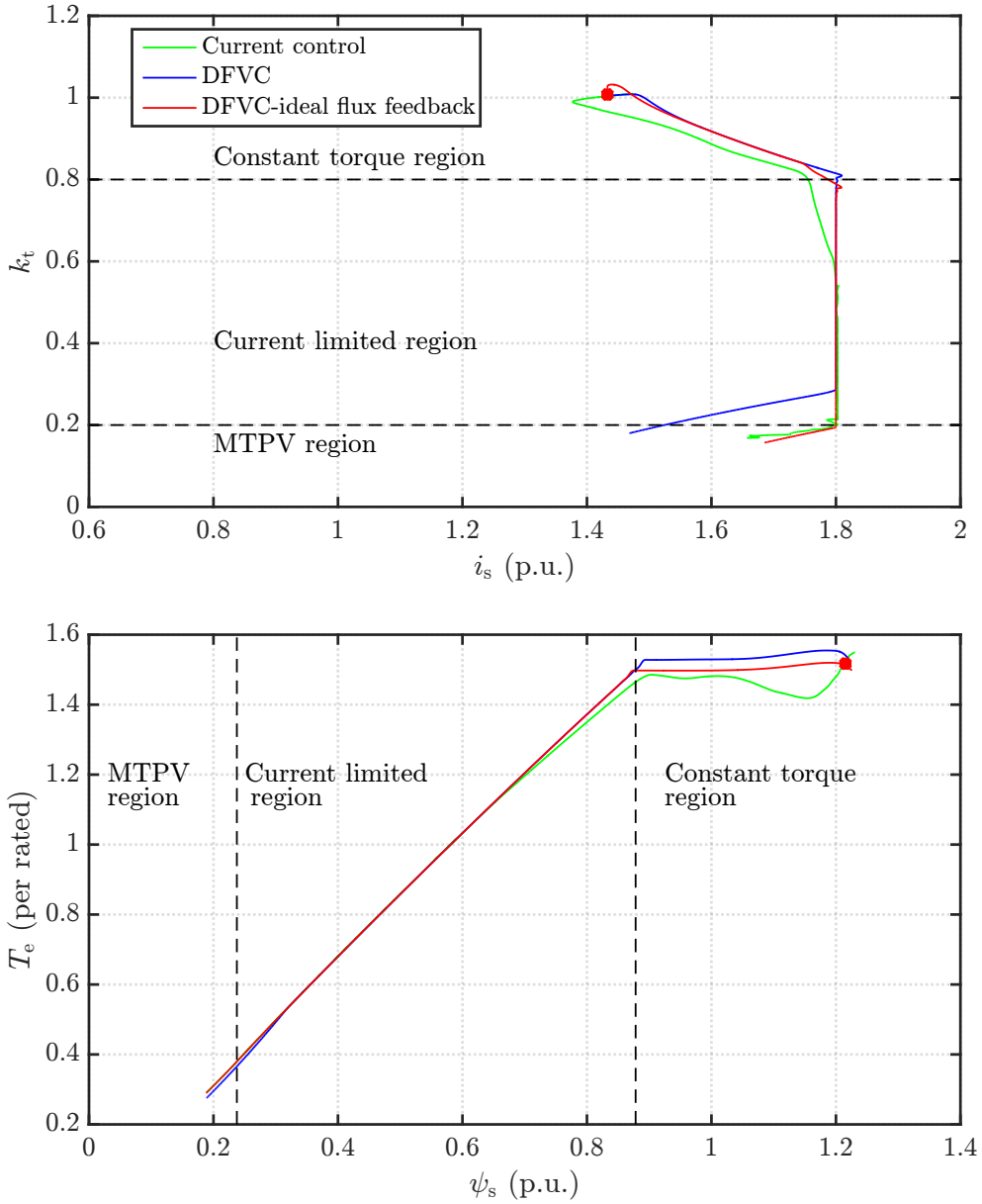

Figure 5.15: Performance comparison of the DFVC with current control approach for $\omega_{m,ref} = 5$ p.u.. The upper subplot shows torque factor against stator current and the lower subplot shows electromagnetic torque against stator flux.

It can be inferred from the results that if the flux information is accurate, the DFVC scheme produces the most optimal results in all regions of operation. The benchmark technique nearly follows the DFVC in the MTPV region. In general terms, the benchmark technique is simple to implement than the DFVC. Firstly, a flux observer is not required and secondly only the controlled variables are needed to be tuned. Comparing with the DFVC in addition to the controlled variables, the tuning of δ-loop is required thus making the control more complicated.

6 Conclusions

In this thesis, the torque maximizing and field weakening control techniques for synchronous machines with magnetically anisotropic structure such as SyRMs and IPMs were studied. MTPA is a control strategy used for efficient motor operation. It is based on obtaining maximum torque with minimal stator current magnitude thus suppressing the copper losses to as low as possible. The FW technique allows the motor to reach higher speeds at a limited supply voltage. Similar to the MTPA the goal in the FW region is to maximize the torque but minimizing the stator flux instead of the stator current. The technique is known as the MTPV control. The drive must operate with these control techniques for the most optimal response whether in terms of minimum loss operation or high speed operation. Physical limitations and non-linear behaviour of the motor which must be taken into account in the control solution.

In this thesis, the optimal control strategies are implemented using the DFVC technique. The DFVC technique is suited for applications designed to operate in FW region. It allows direct control of stator flux by manipulation of the stator flux vector as a controlled variable. The main goal of the thesis is to evaluate the performance of the DFVC in unsaturated and saturated magnetic conditions. The performance criteria is based on how well the DFVC operate with the optimum control techniques. The results of the thesis are divided into five cases. In the first case, simulations are carried out in the speed control mode to simulate the response to the use of a linear magnetic model in the observer and the plant. It was found that the control performance is highly dependent on the accuracy of the estimation performed by the observer. Errors in discretization from continuous-time to discrete-time domain reduces the performance. To determine the robustness of the control scheme a series of load tests were conducted by introducing erroneous parameters in the controller below the cross over frequency of the observer. This was studied as case two. It is found that the DFVC control is highly sensitive to variation in $\hat{L}_{\mathrm{q}}$ and moderately sensitive to $\hat{\psi}_{\mathrm{pm}}$ and nearly insensitive to variation in $\hat{L}_{\mathrm{d}}$ below the crossover frequency. Imprecise model identification results in errors in reference generation and under or overestimation of the flux. Both of these factors increase the stator

current requirement to produce a requested torque compared to one determined by the MTPA control. Case three introduced a saturation model in the plant to accurately simulate the actual motor behaviour. It was found that even though reference torque could not be generated in the constant torque region the motor operates close to optimal in the FW region. Case four introduced the saturation in both the controller and the plant. As a result, optimal results were produced in all regions of operation. In case five, a conventional current vector control scheme was compared with the DFVC. The results yield that the DFVC is the most optimal technique if the flux information is accurate. The current control scheme is as optimal as the DFVC in the MTPV region. The current control technique is trivial in a sense of implementation but requires accurate identification of the motor.

A drawback of the DFVC is the requirement of high switching frequencies for operation as a result of discretization from continuous-time domain. Moreover, the tuning principles for the control are not explicitly defined in the literature. Therefore, a suitable topic for future research would be to derive an exact discrete-time model of the DFVC control scheme. Such a scheme would allow operation at lower switching frequencies. Furthermore, the behaviour of the control scheme could be analysed more precisely.

References

[1] M. Vrazic, D. Vuljaj, A. Pavasovic, and H. Paukovic, "Study of a vehicle conversion from internal combustion engine to electric drive," in *IEEE International Energy Conference (ENERGYCON)*, May 2014, pp. 1544–1548.

[2] G. Pellegrino, E. Armando, and P. Guglielmi, "Direct flux field-oriented control of IPM drives with variable DC link in the field-weakening region," *IEEE Trans. Ind. Appl.*, vol. 45, pp. 1619–1627, Sept 2011.

[3] G. Pellegrino, R. Bojoi, and P. Guglielmi, "Unified direct-flux vector control for AC motor drives," *IEEE Trans. Ind. Appl.*, vol. 47, pp. 2093–2102, Sept 2011.

[4] O. Momoh and M. Omoigui, "An overview of hybrid electric vehicle technology," in *Vehicle Power and Propulsion Conference, 2009. VPPC '09. IEEE*, Sept 2009, pp. 1286–1292.

[5] S. Zhao, "Analysis and control aspects of a PMSynRel drive in a hybrid electric vehicle application," Ph.D. dissertation, KTH Royal Institute of Technology, 2013.

[6] V. T. Buyukdegirmenci, A. M. Bazzi, and P. T. Krein, "Evaluation of induction and permanent-magnet synchronous machines using drive-cycle energy and loss minimization in traction applications," *IEEE Trans. Ind. Appl.*, vol. 50, pp. 395–403, Jan 2014.

[7] P. Sekerak, V. Hrabovcova, J. Pyrhonen, S. Kalamen, P. Rafajdus, and M. Onufer, "Comparison of synchronous motors with different permanent magnet and winding types," *IEEE Trans. Magn.*, vol. 49, pp. 1256–1263, March 2013.

[8] S. M. Taghavi, M. Jain, and S. S. Williamson, "A comparative study of sensorless control techniques of interior permanent magnet synchronous motor drives for electric vehicles," in *IEEE Vehicle Power and Propulsion Conference (VPPC), 2011*, Sept 2011, pp. 1–7.

[9] S. Y. Jung, J. Hong, and K. Nam, "Current minimizing torque control of the IPMSM using ferrari's method," vol. 28, no. 12, pp. 5603–5617, Dec 2013.

[10] M. Bilewski, A. Fratta, L. Giordano, A. Vagati, and F. Villata, "Control of high-performance interior permanent magnet synchronous drives," *IEEE Trans. Ind. Appl.*, vol. 29, pp. 328–337, Mar. 1993.

[11] G. Pellegrino, E. Armando, and P. Guglielmi, "Field oriented control of IPM drives for optimal constant power operation," in *European Conference on Power Electronics and Applications*, Sept. 2007, pp. 1–10.

[12] ——, "Direct-flux field-oriented control of IPM motor drives with robust exploitation of the maximum torque per voltage speed range," in *IEEE International Symposium on Industrial Electronics (ISIE)*, July 2010, pp. 1271–1277.

[13] ——, "Direct-flux vector control of IPM motor drives in the maximum torque per voltage speed range," *IEEE Trans. Ind. Electron.*, vol. 59, no. 10, pp. 3780–3788, Oct. 2012.

[14] G. Pellegrino, B. Boazzo, and T. M. Jahns, "Direct flux control of PM synchronous motor drives for traction applications," in *IEEE Transportation Electrification Conference and Expo (ITEC)*, June 2014, pp. 1–6.

[15] M.Hinkkanen, "S-81.3300 control of electric drives lecture notes," Aalto University, Finland, March 2015.

[16] T. Jahns, G. Kliman, and T. W. Neumann, "Interior permanent-magnet synchronous motors for adjustable-speed drives," *IEEE Trans. Ind. Appl.*, vol. IA-22, no. 4, pp. 738–747, July 1986.

[17] S. Morimoto, Y. Tong, Y. Takeda, and T. Hirasa, "Loss minimization control of permanent magnet synchronous motor drives," *IEEE Trans. Ind. Electron.*, vol. 41, no. 5, pp. 511–517, Oct 1994.

[18] S. Morimoto, M. Sanada, and Y. Takeda, "Wide-speed operation of interior permanent magnet synchronous motors with high-performance current regulator," *IEEE Trans. Ind. Appl.*, vol. 30, no. 4, pp. 920–926, July 1994.

[19] S.-H. Kim and S.-K. Sul, "Voltage control strategy for maximum torque operation of an induction machine in the field-weakening region," *IEEE Trans. Ind. Electron.*, vol. 44, no. 4, pp. 512–518, Aug. 1997.

[20] B.-H. Bae, N. Patel, S. Schulz, and S.-K. Sul, "New field weakening technique for high saliency interior permanent magnet motor," in *Conf. Rec. IEEE-IAS Annu. Meeting*, vol. 2, Oct. 2003, pp. 898–905.

[21] Z. Qu, T. Tuovinen, and M. Hinkkanen, "Inclusion of magnetic saturation in dynamic models of synchronous reluctance motors," in *Proc. ICEM'12*, Marseille, France, Sept. 2012, pp. 994–1000.

[22] S. Guha and N. C. Kar, "A new method of modeling magnetic saturation in electrical machines," in *Canadian Conference on Electrical and Computer Engineering (CCECE)*, May 2006, pp. 1094–1097.

[23] H. Chen, Y. Chen, S. r. Huang, and F. Zhang, "Calculation of inductance of permanent magnet synchronous motor considering permanent magnet flux linkage variation of load conditions," in *IEEE Conference and Expo on Transportation Electrification Asia-Pacific (ITEC Asia-Pacific)*, Aug 2014, pp. 1–6.

[24] W. L. Soong, "Design and modelling of axially laminated interioi permanent magnet motor drives for field-weakening applications," Ph.D. dissertation, University of Glasgow, 1993.

[25] P. Huang, C. y. Miao, H. q. Li, and C. Zhang, "Maximum-torque-per-ampere control of interior permanent magnet synchronous machine applied for hybrid electric vehicles," in *International Conference on Control, Automation and Systems Engineering (CASE)*, July 2011, pp. 1–3.

[26] S. Morimoto, T. Ueno, M. Sanada, A. Yamagiwa, Y. Takeda, and T. Hirasa, "Effects and compensation of magnetic saturation in permanent magnet synchronous motor drives," in *IEEE Trans. Ind. Appl.*, Oct 1993.

[27] G. Pellegrino, A. Vagati, P. Guglielmi, and B. Boazzo, "Performance comparison between surface-mounted and interior PM motor drives for electric vehicle application," *IEEE Trans. Ind. Electron.*, vol. 59, no. 2, pp. 803–811, Feb. 2012.

[28] R. Monajemy and R. Krishnan, "Implementation strategies for concurrent flux weakening and torque control of the PM synchronous motor," in *Thirtieth IAS Industry Applications Conference*, vol. 1, Oct 1995, pp. 238–245.

[29] Y. Jeong, S. Sul, S. Hiti, and K. M. Rahman, "Online minimum-copper-loss control of an interior permanent-magnet synchronous machine for automotive applications," *IEEE Trans. Ind. Appl.*, vol. 42, pp. 1222–1229, Sept. 2006.

[30] J.-M. Kim and S.-K. Sul, "Speed control of interior permanent magnet synchronous motor drive for the flux weakening operation," *IEEE Trans. Ind. Electron.*, vol. 33, no. 1, pp. 43–48, Jan 1997.

[31] R. S. Colby and D. W. Novotny, "An efficiency-optimizing permanent-magnet synchronous motor drive," *IEEE Trans. Ind. Appl.*, vol. 24, pp. 462–469, May 1988.

[32] A. Dianov, K. Young-Kwan, L. Sang-Joon, and L. Sang-Taek, "Robust self-tuning MTPA algorithm for IPMSM drives," in *34th Annual Conference of IEEE on Industrial Electronics (IECON)*, Nov. 2008, pp. 1355–1360.

[33] A. Ahmed, Y. Sozer, and M. Hamdan, "Maximum torque per ampere control for interior permanent magnet motors using DC link power measurement," in *Twenty-Ninth Annual IEEE Applied Power Electronics Conference and Exposition (APEC)*, March 2014, pp. 826–832.

[34] G. Pellegrino, B. Boazzo, and T. Jahns, "Magnetic model self-identification for PM synchronous machine drives," in *International Conference on Optimization of Electrical and Electronic Equipment (OPTIM),2014*, May 2014, pp. 252–260.

[35] R. Vilanova and A. Visioli, *PID Control in the Third Millennium*, 1st ed. Springer London, 2012.

[36] A. Vagati, M. Pastorelli, and G. Franceschini, "High-performance control of synchronous reluctance motors," *IEEE Trans. Ind. Appl.*, vol. 33, no. 4, pp. 983–991, Jul./Aug. 1997.

[37] A. Vagati, M. Pastorelli, G. Franceschini, and V. Drogoreanu, "Digital observer-based control of synchronous reluctance motors," in *IEEE Trans. Ind. Appl.*, vol. 1, Oct. 1997, pp. 629–636.

[38] W. Peters, O. Wallscheid, and J. Bocker, "Optimum efficiency control of interior permanent magnet synchronous motors in drive trains of electric and hybrid vehicles," in *17th European Conference on Power Electronics and Applications (ECCE-Europe)*, Sept 2015, pp. 1–10.